

Doctoral Dissertation

**Photoluminescence and Adsorption Properties of
Nanosheets**

September 2013

Asami Funatsu

Graduate School of Science and Technology

KUMAMOTO UNIVERSITY

PREFACE

Nanosheets can be viewed as a new class of inorganic macromolecules. Their thickness is in the molecular range (about 1nm), while their lateral size ranges from several hundred nanometers to several micrometers. Thus, nanosheets have properties of both the bulk material and molecules. Two dimensional nanosheets have been prepared by exfoliation of layered oxides. Nanosheet has a geometric advantage over other types of particles, because highly oriented films can be easily grown by layer-by-layer and Langmuir-Blodgett (LB) techniques. It is also possible to fabricate superlattice-like films using various nanosheets as building blocks. Nanosheets have shown intriguing and exciting properties for use in electronic, ferromagnetic, photocatalytic, magneto-optical, electrochemical, photoresponsive, and photoluminescence.

In the present study we focus on elucidation of photoluminescence and adsorption properties of novel nanosheets. As oxides, they are chemically robust and are likely to be less susceptible to the photobleaching problems of organic dyes and polymers. In addition, because most of the atoms that constitute the nanosheets are in direct contact with adsorbed chemical species, such as H^+ and OH^- , their luminescence properties are affected by adsorption. Thus, luminescent nanosheets have the potential to be useful not only as materials for next generation optical and electro-optical devices but also as the luminescent probes for chemical and bioanalytical sensors. Moreover, we suggest it about the application to the new field of nanosheets

The thesis is composed of 6 chapters.

- Chapter 1 narrates the general backgrounds, several nanosheets, and application of nanosheets.

- Chapter 2 presents photoluminescence of Eu^{3+} and Tb^{3+} adsorbed on oxide nanosheets. In this chapter, the energy transfer promotion by the coadsorbed H_2O is stronger than the phonon

effect, leading to the increase of the emission intensity in high humidity and water.

- Chapter 3 presents a new easy preparation method for titanium oxide nanosheets using solution process under mild conditions. The prepared nanosheets had $K_{1.1}H_{0.9}Ti_2O_5 \cdot 2.6H_2O$ structure. The drastic enhancement of the Eu^{3+} photoluminescent by $Ti_2O_5^{2-}$ nanosheets occurred even in the solution.

- Chapter 4 presents metal-oxide nanosheets with near-infrared (NIR) luminescent properties were synthesized by the exfoliation of $KL_{a1-x}Nd_xNb_2O_7$ layered perovskite. The nanosheets demonstrate a luminescent band at 1060 nm as a result of the ${}^4F_{3/2} \rightarrow {}^4I_{11/2}$ (Nd^{3+}) transition upon excitation at 808 nm. Organic-surface modification greatly enhanced the luminescence while maintaining a high colloidal stability.

- Chapter 5 presents that increase the thermal and chemical stabilities of trypsinproteolysis activity, trypsin was immobilized on graphene oxide nanosheets (GONSs) by a one-step diimide-activated amidation. The trypsin-immobilized GONS showed significantly higher thermal and chemical stabilities than the free form. After heat treatment(at 50 °C for 6 h), the trypsinGONS retained 80% of its initial activity, but free trypsin retained only 4% of its initial activity.

- Chapter 6 gives the general conclusion of the thesis.

CONTENTS

PREFACE

CHAPTER I

Introduction

1.1. General Background	1
1.2. Nanosheets	1
1.2.1. Metal Oxide Nanosheets	2
1.2.2. Graphene Oxide (GO) Nanosheets	3
1.3. Application of Nanosheets	4
1.3.1. Photoluminescent Nanosheets	5
1.3.2. Lanthanide ion doped Nanosheets	6
1.3.3. Intercalated with Lanthanide ion Nanosheets	7
1.4. Objectives and Scope of this thesis	8
References	

CHAPTER II

Photoluminescence of Eu³⁺ and Tb³⁺ Ions Adsorbed on Oxide Nanosheets

2.1. Introduction	17
2.2. Experiments	18
2.3. Results and Discussion	20
2.4. Conclusion	23
References	

CHAPTER III

Mass Production of Titanium (IV) Oxide Nanosheets by a Soft, Solution Process

3.1. Introduction	32
3.2. Experiments	34
3.3. Results and Discussion	35
3.4. Conclusion	39
References	

CHAPTER IV

Nd³⁺-Doped Perovskite Nanosheets with NIR Luminescence

4.1. Introduction	50
4.2. Experiments	51
4.3. Results and Discussion	52
4.4. Conclusion	56
References	

CHAPTER V

Immobilization of Trypsin on Graphene Oxide Nanosheets for Increased Proteolytic Stability

5.1. Introduction.....	68
5.2. Experiments	69
5.3. Results and Discussion.....	72
5.4. Conclusion	75
References	

CHAPTER VI

Conclusion

General Conclusion.....	82
-------------------------	----

CHAPTER- I

Introduction

1.1 General Background

Nanosheets can be viewed as a new class of nano-scale materials. Their thickness is in the molecular range (about 1nm)¹⁻⁴, while their lateral size ranges from several hundred nanometers to several micrometers. Thus, nanosheets have properties of both the bulk material and molecules. Nanosheets have been synthesized by exfoliation of layered materials (see Figure 1-1.). Exfoliation is reported for various layered compounds having cation-exchange properties: smectite clay minerals,⁵ chalcogenides,⁶ metal phosphates,⁷ and oxide⁸. Nanosheets have great potential for optical,⁹⁻¹⁶ catalytic,¹⁷ electrical,¹⁸ and dielectric¹⁹ applications. Nanosheets is that various nanostructures can be fabricated using them as 2D building block.²⁰⁻²² It is even possible to tailor superlattice-like assemblies, incorporation into the nanosheet galleries a wide range of materials²³⁻²⁵ such as organic molecules, polymers, and inorganic and metal nanoparticles. Sophisticated functionalities or nanodevices may be designed through the selection of nanosheets and combining materials, and precise control over their arrangement at the molecular scale. Thus, in the present study, we focus on elucidation of adsorption abilities and photoluminescence properties of novel nanosheets.

1.2 Nanosheets

Figure 1-3. shows that structure of typical nanosheets. Metal oxide nanosheets (Ti-oxide,¹ Mn-Oxide,²⁶ layered perovskites,⁸ etc), metal sulfides nanosheets (MoS₂,²⁷ etc), layer double hydroxide,²⁸ graphene,²⁹⁻³¹ and graphene oxide.³²⁻³⁵ In particular, we study metal oxide nanosheets and graphene oxide.

1.2.1 Metal Oxide Nanosheets

Metal oxide nanosheets are exceptionally rich in both structural diversity and electronic properties, with potential application in areas ranging from catalysis to electronics. Now, by using the exfoliation approach, it is possible to investigate dozens of different 2D oxide nanosheets in search of new phenomena and applications.

Various nanosheets based on metal oxides have been synthesized by exfoliation the precursor crystals of layered oxides into their elemental layers. The most well-established method of synthesizing oxide nanosheets is the intercalation reaction with bulky guest species such as tetrabutylammonium (TBA) ions. In this approach (Figure1-3.), layered metal oxides such as $\text{Cs}_x\text{Ti}_{(2-x/4)}\square_{x/4}\text{O}_4$ (\square :vacancy),^{1,36} can be used as the starting material for the nanosheet. A common feature of these host compounds is cation-exchange properties involving interlayer alkali metal ions, which are a key to facilitating exfoliation. As a first step to exfoliation, these layered materials are acid-exchanged into protonated forms such as $\text{H}_x\text{Ti}_{(2-x/4)}\square_{x/4}\text{O}_4$, in which the interlayer alkali metal ions can be completely removed under suitable conditions while maintaining the layered structure. The resulting protonic oxides are subsequently exfoliated through reaction with a solution containing TBA ions, producing turbid colloidal suspensions of $\text{Ti}_{(2-x/4)}\square_{x/4}\text{O}_4$ nanosheets. Such an exfoliation process is quite general: exfoliation of the other layered host compounds proceeds in a similar fashion.

Figure 1-5 shows AFM image for $\text{Ti}_{(2-x/4)}\square_{x/4}\text{O}_4$ nanosheet. Their images clearly reveal a sheet-like morphology, which is inherent to the host layer in the parent compounds. The thickness and the standard deviation were about 1.6 nm. The values obtained are nearly comparable to the crystallographic thickness of the host layer in the corresponding parent compounds, supporting the formation of mono-nanosheets. These nanosheets have prompted

many efforts to elucidate their structural properties

1.2.2 Graphene Oxide (GO) Nanosheets

Graphene oxide (GO) has attracted intense interest for its use as a precursor material for the mass production of graphene-based materials, which hold great potential in various applications.

Graphene, an atomic-thick layer of carbon atoms arranged in a honeycomb lattice, draws extensive attention from both the experimental and theoretical communities due to its prominent structural and electrical properties²⁹⁻³¹. Intrinsic graphene is a semi-metal or zero-gap semiconductor that has remarkably high electron mobility, around $200,000\text{cm}^2\text{V}^{-1}\text{s}^{-1}$, arising from its linear energy dispersion with respect to wave vector near the Dirac point. The resistivity of graphene is on the order of $10^{-6}\ \Omega\text{cm}$ and is known as the substrate with lowest resistivity at room temperature. In addition, graphene has large specific surface area ($2,630\text{m}^2\text{g}^{-1}$), good chemical stability, and high sensitivity to electrical perturbations due to its ultra-small thickness. A number of approaches have been employed to synthesize graphene, such as the micromechanical exfoliation of graphite, chemical vapor deposition (CVD), epitaxial growth, chemical intercalation, and the reduction of GO.

GO can be synthesized in large quantities by oxidizing inexpensive graphite powders using strong oxidants (e.g., H_2SO_4 , HNO_3 , KMnO_4 , KClO_3 , NaClO_2) with individual sheets obtained by subsequent gentle exfoliation. Currently, there are three major methods used to synthesize GO from graphite: Hummer and Offeman,³³ Staudenmaier,³⁴ and Brodie.³⁵ GO synthesis that graphite powders are first oxidized into graphite oxide with functional groups spreading across the carbon skeleton, which increase the interlayer spacings and weaken the van der Waals force

between adjacent layers; the as-prepared graphite oxide can then be further sonicated in water to obtain suspensions in which individual GO flakes are stabilized by mutual electrostatic attraction and repulsion. During the oxidation process, graphite powders are exfoliated and broken into layers with increased interlayer distance; the landscape of the sp^2 carbon network is modified with oxygen-containing functional groups, defects, and holes. To date, the atomic structure of GO is still elusive due to its nonstoichiometry, and so far several models have been proposed to study the possible functional groups (epoxy, hydroxyl, carbonyl, and carboxyl) and their arrangements across the carbon plane. The unique transport properties and structure make graphene attractive for a variety of promising applications. For example, graphene can be used as anode materials to improve the efficiency of batteries and as transparent conductive electrodes in solar cell. It could also be a potential candidate for integrated circuits-the smallest transistor (one atom thick, 10 atoms wide) known so far was made of graphene. Other applications of graphene and graphene based materials such as field emitters, hydrogen storage, supercapacitors, gas sensors, and bio-sensors have also been reported.

1.3 Application of Nanosheets

Nanosheets exhibit different physical properties, depending on their composition and structure. A fully exposed surface in nanosheets makes it possible to utilize all surface active. 2D lateral confinement in nanosheets, i.e., the quantum confinement effect, can potentially lead to a significant modification of electronic structures and induce novel physical phenomena. As summarized in Table 1-1, nanosheets have shown intriguing and exciting properties for use in catalytic¹⁷, electrical¹⁸, dielectric,¹⁹ and photoluminescence⁹⁻¹⁶. Herein we study photoluminescent nanosheets.

1.3.1 Photoluminescent Nanosheets

The luminescence of Lanthanide ion has been employed as a luminescence probe, used to sense molecules and/or ions based on their specific luminescence properties, such as large Stokes shifts, sharp emission profiles, or long luminescence lifetimes.³⁷⁻³⁹

As Re ion luminescence probes, Eu^{3+} , Sm^{3+} , Tb^{3+} , and Dy^{3+} have been studied. Although the emission intensities of bare Re ions are weak, the emission intensities increase remarkably after chelate formation with an organic ligand.³⁹⁻⁴¹

Additionally, their luminescence lifetimes become long, allowing time-resolved fluorometry. In addition, it is possible to provide molecular recognition functions specific to the lanthanide complexes by designing a complex structure according to the target chemical species. On the other hand, the organic ligands are likely to be decomposed by oxygen radicals in solution and be susceptible to photobleaching problems. Inorganic luminescent materials containing Re ions, such as oxides, are chemically robust and are likely to be less susceptible to these problems. Nanocrystal phosphors have been studied as materials for biological fluorescent labels.⁴²⁻⁴³ However, there are almost no reports on luminescent oxides containing Re ions to sense small targets such as ions and molecules in aqueous solution. One primary reason for this might be that the size of the above nanocrystal phosphors is too large compared to that of ions and molecules.

Though, many group have reported layered films reassembled from photoluminescent nanosheets (nanosheets of both Re ion doped and intercalated Re ion), because of the expectation for various applications such as photocatalysts, batteries, semiconductor devices, and optical devices.

1.3.2 Lanthanide ion doped nanosheets

Lanthanide ion doped nanosheets are photoluminescent. Such luminescent nanosheets⁹⁻¹⁶ have a geometric advantage in that highly oriented films might be easily fabricated and thus may be promising for next-generation optical and electro-optical devices, as well as for luminescent probes in chemical and biosensors. Luminescent oxide nanosheets usually show distinct excitation and emission behavior from their parent compounds. For example, Eu^{3+} -doped $\text{La}_{0.90}\text{Eu}_{0.05}\text{Nb}_2\text{O}_7$ nanosheets exhibit photoluminescence emission of Eu^{3+} by either direct excitation of Eu^{3+} or host excitation. The most intense emission from $\text{La}_{0.90}\text{Eu}_{0.05}\text{Nb}_2\text{O}_7$ nanosheets is observed by host excitation at the broad excitation band maximum (353 nm).¹³ This is in striking contrast to the bulk $\text{KLa}_{0.90}\text{Eu}_{0.05}\text{Nb}_2\text{O}_7$ precursor, in which direct excitation yields more intense emission than host excitation. Similarly, the most intense emission of $\text{Eu}_{0.56}\text{Ta}_2\text{O}_7$ nanosheets by host excitation exceeds 18 times that from direct Eu^{3+} excitation.¹² The difference in the photoluminescence properties between the nanosheets and their bulk layered compounds seems to be related to the dimensionality of these host structures and the confinement of the energy transfer process between the host layer units and Eu^{3+} activators.

On the other hand, intense red and green emissions are also observed in aqueous suspensions of $\text{Gd}_{1.4}\text{Eu}_{0.6}\text{Ti}_3\text{O}_{10}$ and $\text{La}_{0.7}\text{Tb}_{0.3}\text{Ta}_2\text{O}_7$ nanosheets⁹, respectively. A coincidence in bandgap absorption and excitation spectrum indicates that the visible emission results from energy transfer within the nanosheets. A two-step energy transfer cascade within the $\text{Gd}_{1.4}\text{Eu}_{0.6}\text{Ti}_3\text{O}_{10}$ nanosheet, from the Ti-O host network to Gd^{3+} and then to Eu^{3+} , brings about a much stronger red emission intensity. With intense red-, green-, and blue-emitting¹⁰ Lanthanide ion doped oxide nanosheets being developed, luminescent devices with full chromaticity might be built up entirely with these nanosheets.

1.3.3 Intercalated with Lanthanide nanosheets

Recently, it has been reported that several types of layered oxides and TiO₂ nanoparticles doped with lanthanide cations show strong emission by an energy transfer process from the host matrix excited by band gap illumination to the in-matrix lanthanide cations. This behavior suggests that lanthanide cations in the interlayer of the Ti layered oxides might result in strong emission under the excitation of the host layer, because the host TiO₆ nanosheet layer has a quantum size effect of a large band gap in comparison with the bulk TiO₂. However, only a few papers have been reported for the photoluminescence property of the Ti and Nb layered oxides intercalated with lanthanide cations by the ion-exchange technique, and only weak emission has been observed at 77 K. Recently, we also have reported the photoluminescence of various lanthanide cations in the interlayer of Ti layered oxide.⁴⁴⁻⁴⁶

Eu³⁺ emission of layered titanium oxide intercalated with Eu³⁺ was affected by the amount of interlayer water. Interestingly, the Eu³⁺ emission intensity increased with increasing interlayer water molecules. The red emission of Eu³⁺ was observed under radiation by UV light with an energy higher than the band gap of the host TiO_x layer. The emission is believed to be based on an energy transfer from the host TiO_x layer to Eu³⁺. Although the mechanism remains unclear, the energy transfer was promoted by intercalated water molecules. This indicates that layered titanium oxide intercalated with Eu³⁺ is a good candidate for water-resistant inorganic lanthanide luminescence probes to sense ions and molecules.

1.4 Objectives and scope of this thesis

A most important and attractive aspect of nanosheets is that they are charge-bearing and adsorption behavior. Various nano-architectures, including aggregated flocculates, multilayer thin

films and hollow nanocapsules, can thus be readily fabricated by using the nanosheets as building blocks. It is even possible to tailor superlatticelike composites or hybrid assemblies, incorporating inorganic ions, organic molecules or polymers, and metal nanoparticles as well as nanosheet counterparts. In the present study, we focus on application of nanosheets via adsorption abilities.

Main goal of this study are states as follows;

- Elucidation of comparing with those of some photoluminescent perovskite oxide nanosheets containing Ln^{3+} inside the nanosheet, and the photoluminescence mechanism is discussed.
- Synthesis of novel mono-nanosheets by soft-solution process and photoluminescence properties using their nanosheets.
- Development Nd^{3+} -activated nanosheets with NIR luminescence for bioprobe.
- Preparation of a simple and natural method for enzyme-immobilized GO by the diimideactivated amidation of GO.

References

- (1) T. Sasaki, M. Watanabe, H. Hashizume, H. Yamada, H. Nakazawa, *J. Am. Chem. Soc.*, 1996, 118, 8329.
- (2) R. Abe, K. Shinohara, A. Tanaka, M. Hara, J. N. Kondo, K. Domen, *Chem. Mater.*, 1997, 9, 2179.
- (3) R. E. Schaak, T. E. Mallouk, *Chem. Mater.*, 2000, 12, 2513.
- (4) R. Ma, Z. Liu, K. Takada, N. Iyi, Y. Bando, T. Sasaki, *J. Am. Chem. Soc.*, 2007, 129, 5257.
- (5) T. J. Pinnavaia, *Science*, 1983, 365.
- (6) D. W. C. Murphy, G. W. Hull, Jr., *J. Chem. Phys.*, 1975, 62, 973.
- (7) N. Yamamoto, T. Okuhara, T. Nakato, *J. Mater. Chem.*, 1990, 2, 279.
- (8) M. M. J. Treacy, S. B. Rice, A. J. Jacobson, J. T. Lewandowski, *Chem. Mater.*, 1990, 2, 279.
- (9) S. Ida, C. Ogata, M. Eguchi, W. Justin Youngblood, T. Mallouk, and Y. Matsumoto, *J. Am. Chem. Soc.*, 2008, 130, 7052.
- (10) S. Ida, C. Ogata, U. Unal, K. Izawa, T. Inoue, O. Altuntasoglu, and Y. Matsumoto, *J. Am. Chem. Soc.*, 2007., 129, 8956.
- (11) S. Ida, Y. Sonoda, and Y. Matsumoto, *J. Ceramic. Process. Res.*, 2011, 12, s17.
- (12) T. Ozawa, K. Fukuda, K. Akatsuka, Y. Ebina, T. Sasaki, K. Kurashima, and K. Kosuda, *J. Phys. Chem.C.*, 2008, 112, 1312.
- (13) T. Ozawa, K. Fukuda, K. Akatsuka, Y. Ebina, and T. Sasaki, *Chem. Meter.*, 2007, 19, 6575.
- (14) K-H Lee, B-I Lee, J-H You and S-H Byeon, *Chem. Commun.*, 2010, 1461.
- (15) T. Sasaki, M. Watanabe, *J. Phys. Chem. B.*, 1997, 101, 10159.
- (16) M. Osada, T. Sasaki, K. Ono, Y. Kotani, S. Ueda, and K. Kobayashi, *ACS Nano.*, 2011, 5, 6871.

- (17) Y. Ebina, T. Sasaki, M. harada, and M. Watanabe, *Chem. Mater.*, 2002, 14, 4390.
- (18) B-W. Li, M. Osada, T. C. Ozawa, Y. Ebina, K. Akatsuka, R. Ma, H. Funakubo, and T. Sasaki, *ACS. Nano.*, 2010, 4, 6673.
- (19) M. Osada, T. Sasaki, *J. Appl. Ceram. Technol.*, 2012, 9, 29.
- (20) T. Sasaki, *J. Ceram. Soc. Jpn.* 2007, 115, 9.
- (21) M. Osada, T. Sasaki, *J. Mater. Chem.* 2009, 19, 2503.
- (22) S. W. Keller, H.-N. Kim, T. E. Mallouk, *J. Am. Chem. Soc.*, 1994, 116, 8817.
- (23) L. Z. Wang, Jr., Y. Omomo, N. Sakai, K. Fukuda, I. Nakai, Y. Ebina, K. Takada, M. Watanabe, T. Sasaki, *Chem. Mater.*, 2003, 15, 2873.
- (24) Y. Umemura, E. Shinohara, A. Koura, T. Nishioka, T. Sasaki, *Langmuir.*, 1979, 101, 334.
- (25) T. Yui, T. Tsuchino, T. Itoh, M. Ogawa, Y. Fukushima, K. Takagi, *Langmuir.*, 2005, 21, 2644.
- (26) Z.-H. Liu, K. Ooi, H. Kanoh, W.-P. Tang, T. Tomida, *Langmuir.*, 2000, 16, 4154.
- (27) J. N. Coleman, M. Lotya, A. O'Neill, A. et al. *Science.*, 2011, 331, 568.
- (28) L. Li, R. Ma, Y. Ebina, N. Iyi, T. Sasaki, *Chem. Mater.*, 2005, 17, 4386.
- (29) A.K.Geim, K. S. Novoselov, *Nat. Mater.*, 2007, 6, 183.
- (30) C. Lee, X. Wei, J. W. Kysar, J. Hone, *Science.* 2008, 321, 385.
- (31) A. A. Balandin, S. Ghosh, W. Bao, I. Calizo, D. Teweldebrhan, F. Miao, C. N. Lau, *Nano Lett.* 2008, 8, 902.
- (32) Y. Matsumoto, M. Koinuma, S. Ida, S. Hayami, T. Taniguchi, K. Hatakeyama, H. Tateishi, Y. Watanabe, and S. Amano, *J. Phys. Chem. C.*, 2011, 115, 19280.
- (33) W. S. Hummers, R. E. Offeman, *J. Am. Chem. Soc.*, 1958, 80, 1339.
- (34) J. R. Lomeda, C. D. Doyle, D. V. Kosynkin, W. F. Hwang, J. M. Tour, *J. Am. Chem. Soc.*,

2008, 130, 16201.

(35) H. K. Jeong, Y. P. Lee, R. Lahaye, M. H. Park, K. H. An, I. J. Kim, C. W. Yang, C. Y. Park, R. S. Ruoff, Y. H. Lee, *J. Am. Chem. Soc.*, 2008, 130, 1362.

(36) Y. Matsumoto, A. Funatsu, D. Matsuo, U. Unal, *J. Phys. Chem. B.*, 2011, 105, 10893.

(37) H. Tsukube, S. Shinoda, H. Tamiaki, *Coord. Chem. Rev.*, 2002, 226, 227.

(38) D. Parker, *Coord. Chem. Rev.*, 2000, 205, 109.

(39) A. P. de Silva, H. Q. N. Gunaratne, T. E. Rice, *Angew. Chem., Int. Ed. Engl.*, 1996, 35, 2116.

(40) S. Petoud, S. M. Cohen, J.-C. G. Bunzli, K. N. Raymond, *J. Am. Chem. Soc.*, 2003, 125, 13324.

(41) R. S. Dickins, J. A. K. Howard, C. L. Maupin, J. M. Moloney, D. Parker, J. P. Reihl, G. Siligardi, J. A. G. Williams, *Chem.-Eur. J.*, 1999, 5, 1095.

(42) P. Schuetz, F. Caruso, *Chem. Mater.*, 2002, 14, 4509.

(43) G. Yi, H. Lu, S. Zhao, Y. Ge, W. Yang, D. Chen, L.-H. Guo, *Nano Lett.*, 2004, 4, 2191.

(44) Y. Matsumoto, U. Unal, Y. Kimura, S. Ohashi, K. Izawa, *J. Phys. Chem. B* 2005, 109, 12748.

(45) S. Ida, U. Unal, K. Izawa, O. Altuntasoglu, C. Ogata, T. Inoue, K. Shimogawa, Y. Matsumoto, *J. Phys. Chem. B* 2006, 110, 23881.

(46) S. Ida, C. Ogata, Y. Matsumoto, *J. Phys. Chem. B* 2009, 113, 1896.

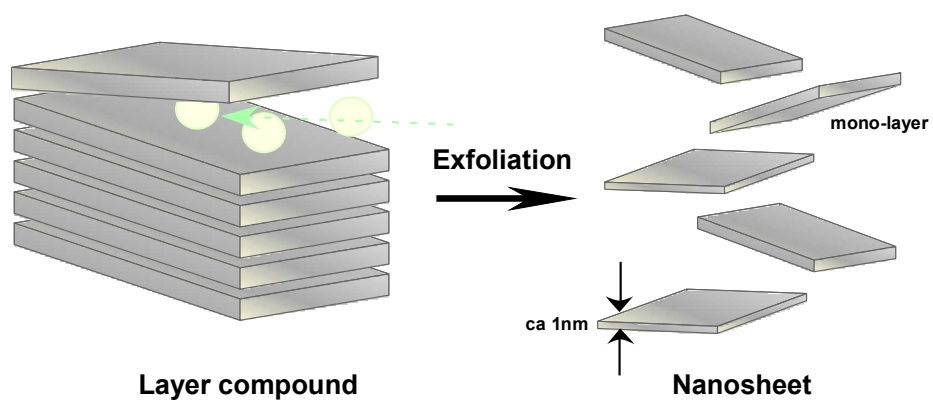


Figure 1-1 . Exfoliation process of Layer compound

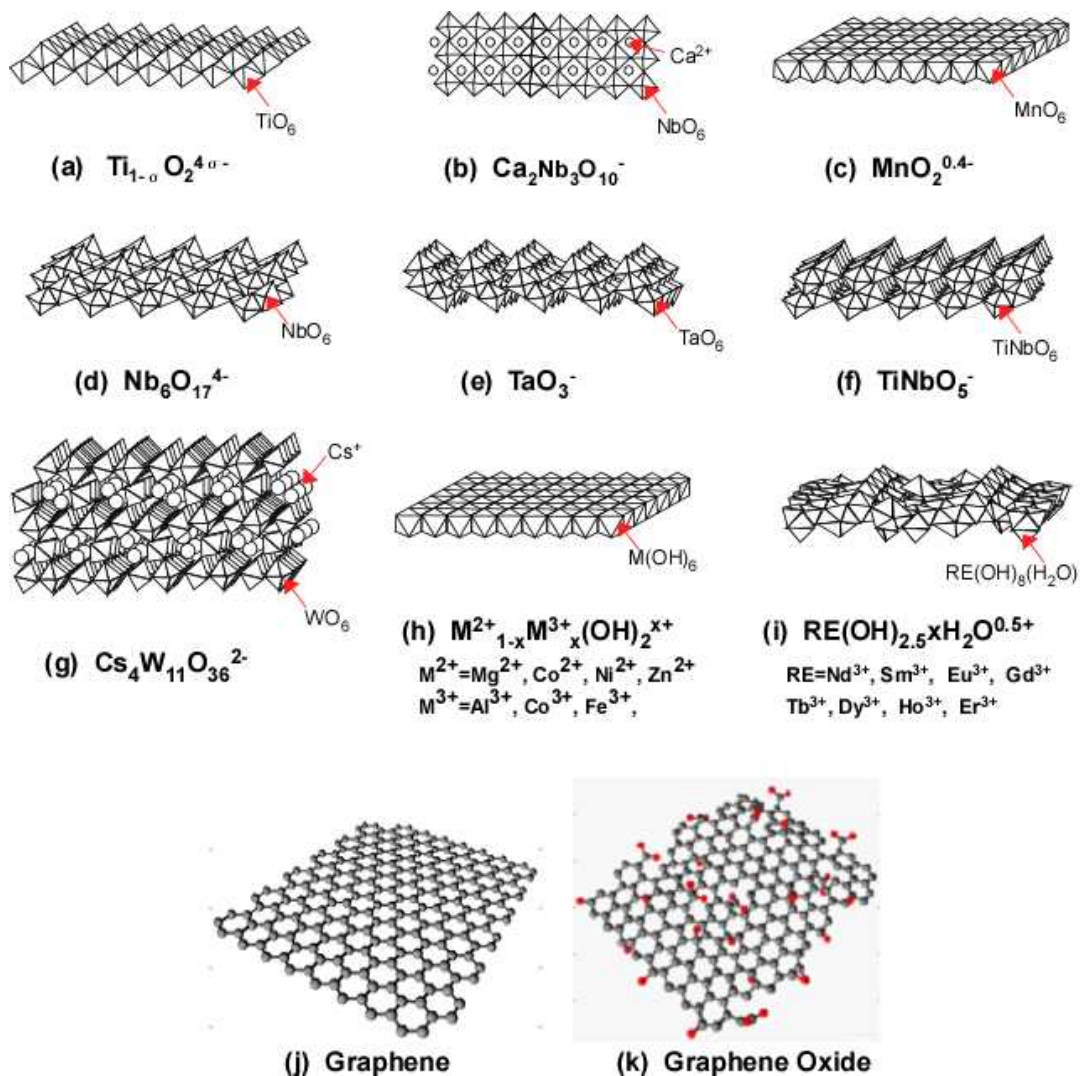


Figure 1-2. Structure of typical nanosheets.

(a) Titanium oxide, (b) calcium niobium oxide, (c) manganese oxide, (d) niobium oxide, (e) tantalum oxide, (f) titanium niobium oxide, (g) cesium tungsten oxide, (h) Layered double hydroxide, (i) layered rare-earth hydroxide, (j) graphene, and (k) graphene oxide.

Table 1.1 Classification of physical properties in nanosheets

Materials		Properties
Type	Composition	
Ti oxide	$\text{Ti}_{1-x}\text{O}_{2^{4x-}}$, $\text{Ti}_{0.91}\text{O}_{2^{0.36-}}$, $\text{Ti}_{0.87}\text{O}_{2^{0.52-}}$	Photocatalytic, Dielectric
	$\text{Ti}_{0.8}\text{Co}_{0.2}\text{O}_{2^{0.4-}}$, $\text{Ti}_{0.6}\text{Fe}_{0.4}\text{O}_{2^{0.4-}}$	Ferromagnetic
Mn oxide	$\text{MnO}_{2^{-}}$	Redoxable
Nb/(Ti) and Ta oxide	$\text{Nb}_6\text{O}_{17^{4-}}$, $\text{Nb}_3\text{O}_8^{-}$, TiNbO_5^{-} , $\text{Ti}_2\text{NbO}_7^{-}$,	Photocatalytic, Dielectric
	$\text{Ti}_5\text{NbO}_{14^{3-}}$, TaO_3^{-}	
Perovskite oxide (Ti, Nb, Ta)	$\text{RE}_2\text{Ti}_3\text{O}_{10^{2-}}$ (RE: La, Pr, Sm, Nd, Eu, Gd, Tb, Dy)	Photocatalytic, Dielectric, Photoluminescent
	$\text{Ca}_2\text{Nb}_3\text{O}_{10^{-}}$, $\text{Gd}_{1.4}\text{Eu}_{0.6}\text{Ti}_3\text{O}_{10^{2-}}$	
W oxides	$\text{W}_2\text{O}_7^{2-}$, $\text{Cs}_4\text{W}_{11}\text{O}_{36}^{2-}$	Redoxable, Photochromic
LDH	$[\text{M}^{2+}_{1-x}\text{Al}^{3+}_x(\text{OH})_2]_x^+$ (M: Mg, Co, Ni, Zn) ($0.2 \leq x \leq 0.33$)	Redoxable, Magnetic
Graphene	-	optical, semiconducting(zero-band-gap), etc
Graphene oxide	-	Photoluminescent, electrochemical etc

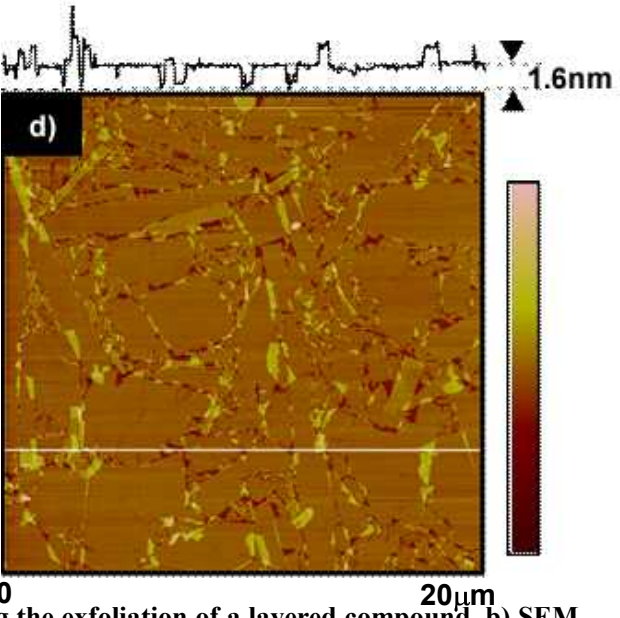
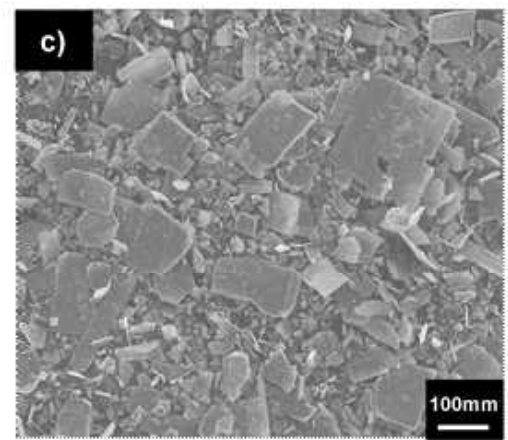
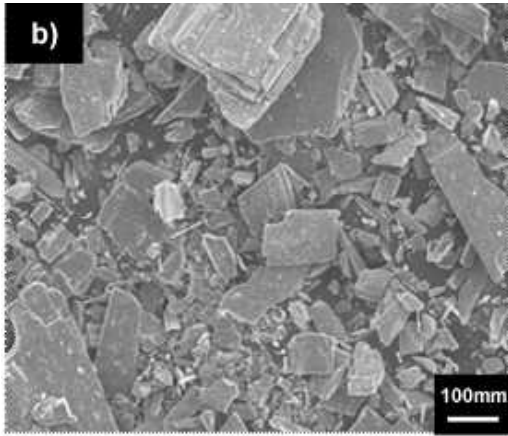
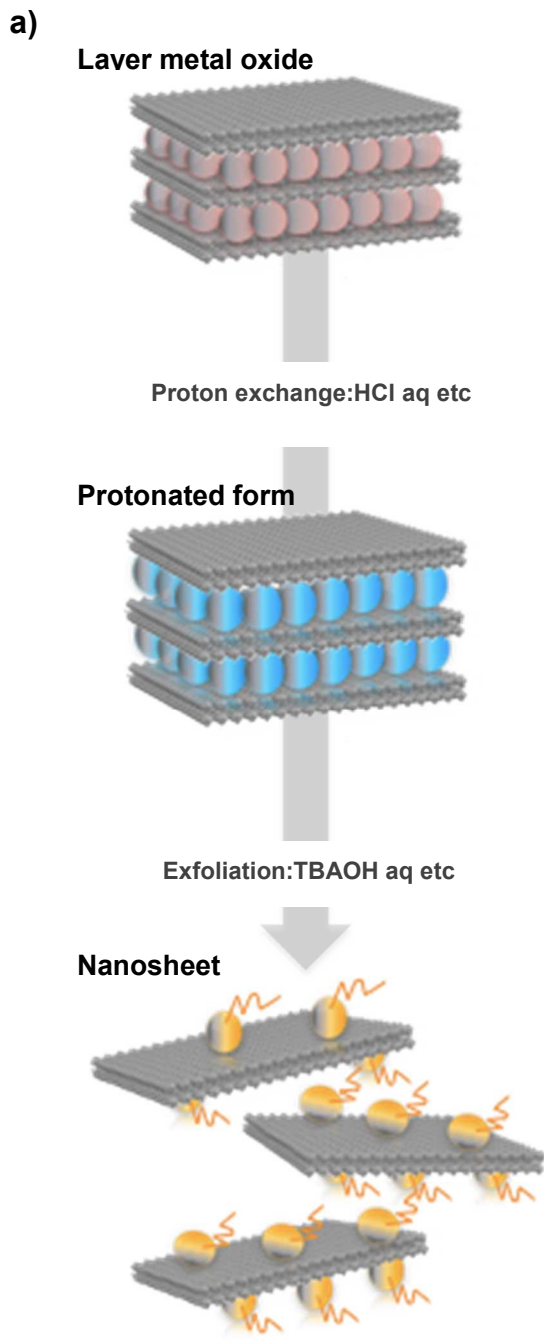


Figure 1-3. (a) Schematic model illustrating the exfoliation of a layered compound, (b) SEM image of layer metal oxide. (c) SEM image of protonated form and AFM image of nanosheets.

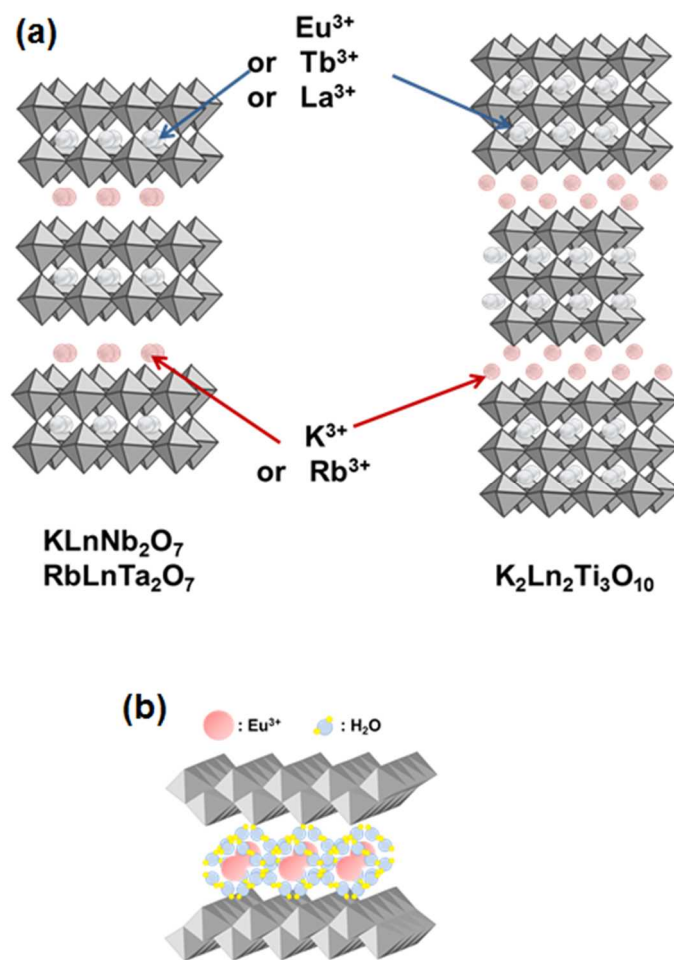


Figure 1-4. (a) Structure model of Re ion doped nanosheets precursors. (b) Structure model of Re ion intercalated nanosheets precursor.

CHAPTER-II

Photoluminescence of Eu^{3+} and Tb^{3+} Ions Adsorbed on Oxide Nanosheets

Overview

Photoluminescence properties of TiO ($\text{Ti}_{1.825}\text{O}_4$) and NbO (Nb_6O_{17}) nanosheets adsorbed with Ln^{3+} ions were studied comparing with those of photoluminescent GdEuTiO and LaTbTaO perovskite nanosheets. Intense emissions of Ln^{3+} (Eu^{3+} and Tb^{3+}) ions adsorbed on TiO and NbO (Ln^{3+}/MO) nanosheets were observed during UV light illumination. The photoluminescence results from the energy transfer from the band gap excitation of the nanosheets to the adsorbed Ln^{3+} . Coadsorbed H_2O increased the emission intensities of the adsorbed Ln^{3+} for the Ln^{3+}/MO samples. On the other hand, no effect of adsorbed H_2O on the emission intensities of the photoluminescent perovskite nanosheets was observed because of the presence of Ln^{3+} on the inside of the nanosheets. Hydrogen-bonding networks between O^{2-} ions of the nanosheet surface and the adsorbed H_2O surrounding Ln^{3+} will promote the energy transfer for the Ln^{3+}/MO samples. Recombination and photoreaction of the produced electron and hole of the nanosheet, and a phonon due to the adsorbed H_2O suppress the emission, according to the analyses of effects of pH, adsorbed ions and D_2O on the emission.

2.1 Introduction

Semiconducting oxide nanosheets such as TiO, NbO, and TaO nanosheets, have many promising properties such as photoluminescence,¹⁻⁸ photocatalysis,⁹⁻¹¹ electrochemistry,^{12,13} and so on.¹⁴ In addition, nanosheets might show a peculiar reaction in the presence of Ln^{3+} .¹⁵ In particular, many unique properties concerning photoluminescence have been reported as follows.

- 1) The photoluminescence of Ln^{3+} results mainly from an energy transfer from the

nanosheet band gap excitation to the Ln^{3+} .^{1,3-8}

- 2) Adsorbed or absorbed H_2O promotes the energy transfer to bring about intense emission, especially for $\text{Eu}^{3+}/\text{TiO}$ systems.⁵
- 3) The emission intensity depends on solution pH. Usually, the intensity decreases at low pH.⁴

The above photoluminescence properties have been observed for Ln^{3+} intercalated layered oxides with $\text{MO}/\text{Ln}^{3+}/\text{MO}$ ($\text{M} = \text{Ti}, \text{Nb}, \text{and Ta}$) sandwich structure^{4,5} and some perovskite oxide nanosheets with Ln^{3+} in the A site.^{1,3}

Here, we report an intense emission in the photoluminescence of Ln^{3+} adsorbed on the oxide nanosheets, i.e., Ln^{3+}/MO . In this paper, various photoluminescence properties of Ln^{3+}/MO are demonstrated comparing with those of some photoluminescent perovskite oxide nanosheets containing Ln^{3+} inside the nanosheet, and the photoluminescence mechanism is discussed.

2.2 Experimental

Materials.

In this study, we used some oxide nanosheets such as $\text{Ti}_{1.825}\text{O}_4$ (TiO), Nb_6O_{17} (NbO), $\text{Gd}_{1.4}\text{Eu}_{0.6}\text{Ti}_3\text{O}_{10}$ (GETiO), and $\text{La}_{0.7}\text{Tb}_{0.3}\text{Ta}_2\text{O}_7$ (LTTaO). These nanosheets (nanosheet solutions) were prepared by the same methods as reported in previous papers.^{1,5} It was proven from the nanosheet thickness measured by atomic force microscopy, that the nanosheets exist as mono-nanosheet (0.84nm for TiO, 1.03 nm for NbO, 2.4nm for GETiO, and 1.8 nm for LTTaO).

Preparation of Mono-Nanosheet Films.

The nanosheets were attached on a quartz substrate layer by layer (LBL) as follows. A

quartz plate was used as a substrate in this study. Substrates were primed in 2.5 g L⁻¹ aqueous poly(ethyleneimine) (PEI) solution for 20min to charge the surface of the substrates positively. Primed substrates were dipped into a colloidal solution with negatively charged MO (M = Ti, Nb, Ta, GETi, and LTTa) nanosheets. Mono-nanosheet films were formed on the substrate surfaces for all the samples.

Preparation of Ln³⁺-Adsorbed Oxide Nanosheets.

The quartz substrates covered with mono-nanosheets were immersed in a solution containing Eu³⁺ or Tb³⁺ ions (1×10^{-2} M Ln(CH₃COO)₃) for 20min, and then immersed in pure water for 30 s. The samples were dried under pure N₂ at room temperature. The Ln³⁺ adsorbed on the oxide nanosheets prepared by the above simple process are represented as Ln³⁺/MO in this paper.

Photoluminescence Measurement.

Figure 2-1 shows a schematic illustration of the system used for the measurement of the photoluminescence. Excitation and emission spectra were analyzed with a Jasco FP-6500 spectrofluorometer with a 150W Xe lamp source. Excitation and emission spectra of Ln³⁺/MO films were prepared, the films were put in a triangle quartz cell filled with several aqueous solutions (aqueous solution, aqueous metal ion solution, and aqueous methanol solution).

Characterization and Equipment.

The amount of the adsorbed Ln³⁺ was analyzed by means of an inductively coupled plasma

(ICP) spectrophotometer (SEIKO Instruments, SPS7800). The emission decay curves were plotted on the basis of the time-resolved emission spectra, which were obtained by using a Perkin-Elmer LS 55 fluorescence spectrometer.

2.3 Results and Discussion

Adsorbed H₂O Effect.

Figures 2-2a and 2-2b show photoluminescence spectra of the Eu³⁺/TiO and Tb³⁺/NbO in pure water respectively. Intense characteristic emissions of the adsorbed Ln³⁺ appeared. Both the emissions result from the energy transfer from the band gap excitation of the oxide nanosheets to the adsorbed Ln³⁺, judging from the excitation spectra. On the other hand, no such intense emission was observed for polycrystalline TiO₂ particle film such as P25 (consisting of about 20 nm particles) on which Eu³⁺ was adsorbed. Thus, the nanosheet with special structure is necessary for the present intense emissions of the adsorbed Ln³⁺. The photoproduced electron and hole separately exist in the inside and on the nanosheet surface respectively,¹⁴ while those closely exist to bring about easy surface recombination at the polycrystalline particle surface, leading to no energy transfer.

Figures 2-2c and 2-2d show photoluminescence spectra of the Eu³⁺/TiO and Tb³⁺/NbO in air respectively, where relative humidity (RH) was changed by setting a cell containing various H₂SO₄/H₂O solutions in the measurement chamber. The emission intensity increased with the increase of RH for both the samples. This (together with the results in Figures 2-2c and 2-2d) indicates that the energy transfer from the nanosheet band gap excitation to the adsorbed Ln³⁺ is promoted by the coadsorbed H₂O on the surface. As a matter of course, no effect of the adsorbed H₂O was observed for either the GETiO or LTTaO nanosheets, because the Ln³⁺ exists on the

inside of the nanosheets and therefore H₂O in air does not directly attach to the Ln³⁺.

D₂O Effect.

Figures 2-3a and 2-3b show photoluminescence spectra of the Eu³⁺/TiO and Tb³⁺/NbO in D₂O and H₂O solutions respectively. Emission intensities in D₂O stronger than those in H₂O were observed for both the samples. The lifetimes calculated from the decay curves shown in Figures 3c and 3d were longer in D₂O than in H₂O for both the samples (The lifetimes in D₂O and H₂O were 0.99 and 0.23 ms for the Eu³⁺/TiO respectively, and those in D₂O and H₂O were 1.24 and 0.50 ms for the Tb³⁺/NbO respectively.).

It is known that, in general, the excited states relax via two competitive paths. One is by light emission, and the other is by phonon emission (radiationless quenching); the latter path applies to the present case. The rate of phonon emission, ω , depends on the phonons simultaneously emitted to bridge the energy gap, and is expressed as

$$\omega \propto \exp(-k\Delta E/h\nu_{\max}) \quad (1)$$

Where ΔE is the energy gap to the nearest lower level and $h\nu$ is the maximum energy of phonons coupled to the emitting state^{16,17} The phonon emission rate, ω , decreases rapidly with increasing ΔE , so that the competitive light emission or radiative process becomes dominant. Large values of $h\nu_{\max}$ also quench light emission. Therefore, in general, the photoluminescence of Ln³⁺ ions strongly depends on the chemical environment of the ions, and Ln³⁺ ions exhibit a stronger luminescence in D₂O than in H₂O because of the smaller phonon energy of D₂O ($\nu_{\text{O-D, stretch, max}} \sim 2800 \text{ cm}^{-1}$) than that of H₂O ($\nu_{\text{OH, stretch, max}} \sim 3600 \text{ cm}^{-1}$).¹⁸ This indicates that the general quenching effect of Ln³⁺ emission by H₂O occurs in the interlayer of Ln³⁺/MO. Thus, the photoluminescence properties of Ln³⁺/MO films are dependent on the hydration state of the

water molecules surrounding the Ln^{3+} ions in the interlayer, as occurs in general with Ln^{3+} ions in aqueous solution. From the lifetimes of Ln^{3+} in H_2O and D_2O , it is possible to evaluate the number of water molecules directly coordinated to interlayer Ln^{3+} , q^{Ln} , by the following equation:

$$q^{\text{Eu}} = 1.2[(1/\tau_{\text{HEu}}) - (1/\tau_{\text{DEu}}) - 0.25] \quad (2)$$

$$q^{\text{Tb}} = 5.0[(1/\tau_{\text{HTb}}) - (1/\tau_{\text{DTb}}) - 0.06] \quad (3)$$

Where τ_{HLn} and τ_{DLn} are luminescence lifetimes of Ln^{3+} in H_2O or D_2O , respectively.¹⁹⁻²²

Thus the Eu/TiO film has 3.7 inner sphere water molecules, and the Tb/NbO film has 5.7 inner sphere water molecules.

pH Effect.

Figures 2-4a and 2-4b show pH dependences of the emission intensities of the $\text{Eu}^{3+}/\text{TiO}$ and $\text{Tb}^{3+}/\text{NbO}$ respectively. The intensity for the $\text{Eu}^{3+}/\text{TiO}$ decreased at low pH, while that for the $\text{Tb}^{3+}/\text{NbO}$ decreased at high pH. Similar pH dependences of the emission intensities of the GETiO and LTTaO samples were observed as shown in Figures 4c and 4d respectively, although the effects were small. The following two mechanisms can be surmised for the pH dependence.

1) The recombination between the produced hole and electron will be promoted at low pH. The photoproduced electron and hole exist inside the nanosheet and on the surface O^{2-} respectively.¹⁴ Adsorbed H^+ on the surface at low pH will push the hole from the surface to the inside and attract the electron from the inside to the surface by electrostatic force, and therefore the recombination will be promoted to suppress the energy transfer at low pH. This effect will be pronounced for the Ti oxide nanosheets (Figures 2-4a and 2-4c).

2) The bonding state of the adsorbed H_2O surrounding Ln^{3+} for the Ln^{3+}/MO samples will

be changed by pH. At high pH, the number of H₂O molecule surrounding Ln³⁺ increases, resulting in the increase of the energy transfer. This effect will be pronounced for the Tb³⁺/NbO (Figure 4b). As previously explained a difference of number of the inner sphere water molecules affects the emission of light in Eu/TiO and Tb/NbO.

Other Ions and Solvent Effects.

Figure 2-5 shows effects of added Co²⁺, Ag⁺, and CH₃OH on the photoluminescence spectra. The addition of transition-metal cations such as Co²⁺ and Ag⁺ (2.5×10^{-2} M) brought about a decrease in the emission intensities for all the Ln³⁺/MO samples (Figures 2-5a and 2-5b). This is due to photoreaction (photodeposition) leading to consumption of the photoproduced electron and hole. As a result, the energy transfer decreases to bring about a decrease in the emission intensity. Table 2-1 shows the quantity of each ion (Ln³⁺) of several aqueous solutions after immersing samples for five minutes. It was found that ion exchange occurred to the greatest degree in water, however the very small degree to which it occurred did not affect the emission.

CH₃OH brought about change in the emission intensity (Figures 2-5c and 2-5d). Two mechanisms can be rationalized. One as in the case of Co²⁺ and Ag⁺ adsorptions, is photooxidation of alcohol. The other is the decrease of the amount of adsorbed H₂O on the nanosheet surface in alcohol solutions. These will bring about a decrease in the emission intensity as in the case of Eu³⁺/Ti (Figure 5c). However, the increase in the intensity for Tb³⁺/NbO suggests direct promotion by CH₃OH of the emission. Consequently, the change of the emission intensity by addition of transition-metal ions and alcohol suggests that the Ln³⁺/MO will act as a sensor using photoluminescence to analyze ions and organic molecules in solution.

2.4 Conclusion

Intense emissions of Ln³⁺ ions (Eu³⁺ and Tb³⁺) adsorbed on TiO and NbO nanosheets were observed. This photoluminescence results from the energy transfer from the band gap excitation of the nanosheets to the adsorbed Ln³⁺. Coadsorbed H₂O increased the emission intensities of the adsorbed Ln³⁺. Hydrogen-bonding networks between O²⁻ ions of the nanosheet surface and the adsorbed H₂O surrounding Ln³⁺ will promote the energy transfer for Ln³⁺/MO. The intensity increased in D₂O because of the decrease of phonon effect of coadsorbed water molecules. Consequently, the energy transfer promotion by the coadsorbed H₂O is stronger than the phonon effect, leading to the increase of the emission intensity in high humidity and water. The emission intensity of the Eu³⁺/TiO and the Tb³⁺/NbO, while Co²⁺ and Ag⁺ addition decreased the emission intensity because the photoproduced electron and hole in the nanosheets are consumed by photoelectrochemical reactions.

References

- (1) S. Ida, C. Ogata, M. Eguchi, W. J. Youngblood, T. E. Mallouk, Y. Matsumoto, *J. Am. Chem. Soc.*, 2008, 130, 7052.
- (2) S. Ida, C. Ogata, U. Unal, K. Izawa, T. Inoue, O. Altuntasoglu, Y. Matsumoto, *J. Am. Chem. Soc.*, 2007, 129, 8956.
- (3) T. C. Ozawa, K. Fukuda, K. Akatsuka, Y. Ebina, T. Sasaki, K. Kurashima, K. Kosuda, *J. Phys. Chem. C* 2008, 112, 1312.
- (4) S. Ida, C. Ogata, Y. Matsumoto, *J. Phys. Chem. C* 2009, 113, 1896.
- (5) Y. Matsumoto, U. Unal, Y. Kimura, S. Ohashi, K. Izawa, *J. Phys. Chem. B* 2005, 109, 12748.
- (6) Layered Oxides Intercalated with Rare Earth Prepared by ESD Method; Book of Abstracts No. 45; Rare Earths '04 in Nara, Japan, ed. by N. Imanaka, The Rare Earth Society of Japan, November 2004.
- (7) H. Xin, R. Ma, L. Wang, Y. Ebina, K. Takada, T. Sasaki, *Appl. Phys. Lett.*, 2004, 85, 4187.
- (8) S. Ida, C. Ogata, D. Shiga, K. Izawa, K. Ikeue, Y. Matsumoto, *Angew. Chem., Int. Ed.*, 2008, 47, 2480.
- (9) U. Unal, Y. Matsumoto, N. Tamoto, M. Koinuma, M. Machida, K. Izawa, *J. Solid State Chem.*, 2006, 179, 33.
- (10) O. C. Compton, F. E. Osterloh, *J. Phys. Chem. C* 2009, 113, 479.
- (11) K. Maeda, M. Eguchi, W. J. Youngblood, T. E. Mallouk, *Chem. Mater.*, 2008, 20, 6770.
- (12) K. Izawa, T. Yamada, U. Unal, S. Ida, O. Altuntasoglu, M. Koinuma, Y. Matsumoto, *J. Phys. Chem. B* 2006, 110, 4645.
- (13) K. Akatsuka, Y. Ebina, M. Muramatsu, T. Sato, H. Hester, D. Kumaresan, R. H. Schmehl, T. Sasaki, M. Haga, *Langmuir*, 2007, 23, 6730.

- (14) Y. Matsumoto, S. Ida, T. Inoue, *J. Phys. Chem. C* 2008, 112, 11614.
- (15) O. Altuntasoglu, Y. Matsuda, S. Ida, Y. Matsumoto, *Chem. Mater.*, 2010, 22, 3158.
- (16) Phosphor Handbook, ed. by S. Shionoya, W. M. Yen, CRC Press LCC, Boca Raton, FL, 1999, p. 179.
- (17) L. A. Riseberg, H. W. Moots, *Phys. Rev.*, 1968, 174, 429.
- (18) J. L. Kropp, M. W. Windsor, *J. Chem. Phys.*, 1965, 42, 1599.
- (19) A. Beeby, I. M. Clarkson, R. S. Dickins, S. Faulkner, D. Parker, L. Royle, A. S. de Sousa, J. A. G. Williams, M. Woods, *J. Chem. Soc., Perkin Trans. 2* 1999, 493.
- (20) R. M. Supkowski, W. D. Horrocks, Jr., *Inorg. Chim. Acta.*, 2002, 340, 44.
- (21) W. D. Horrocks, Jr., D. R. Sudnick, *Acc. Chem. Res.*, 1981, 384, 14.
- (22) W. D. Horrocks, Jr., D. R. Sudnick, *J. Am. Chem. Soc.*, 1979, 101, 334.

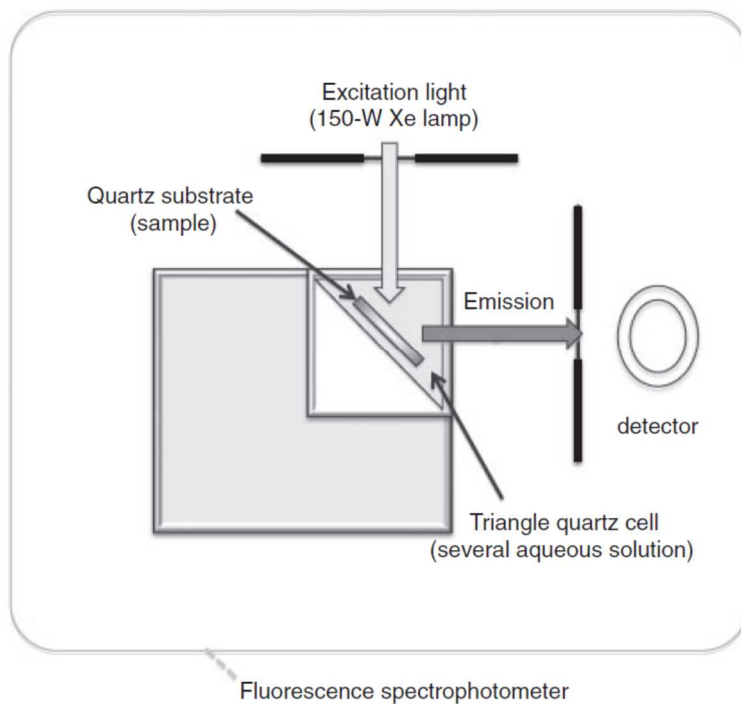


Figure 2-1. Schematic illustration of method used for the measurement of the photoluminescence.

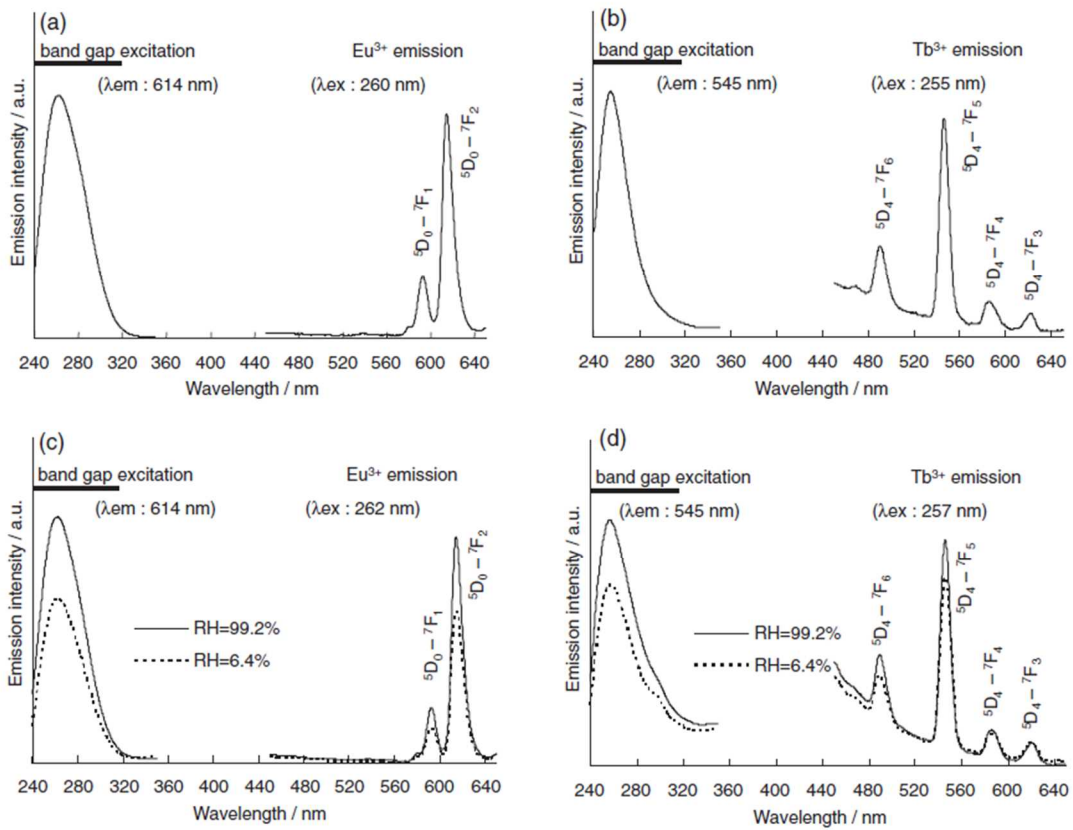


Figure 2-2. Photoluminescence spectra of the Eu³⁺/TiO (a and c) and Tb³⁺/NbO (b and d) in water (a and b) and air with relative humidities (RH) (c and d).

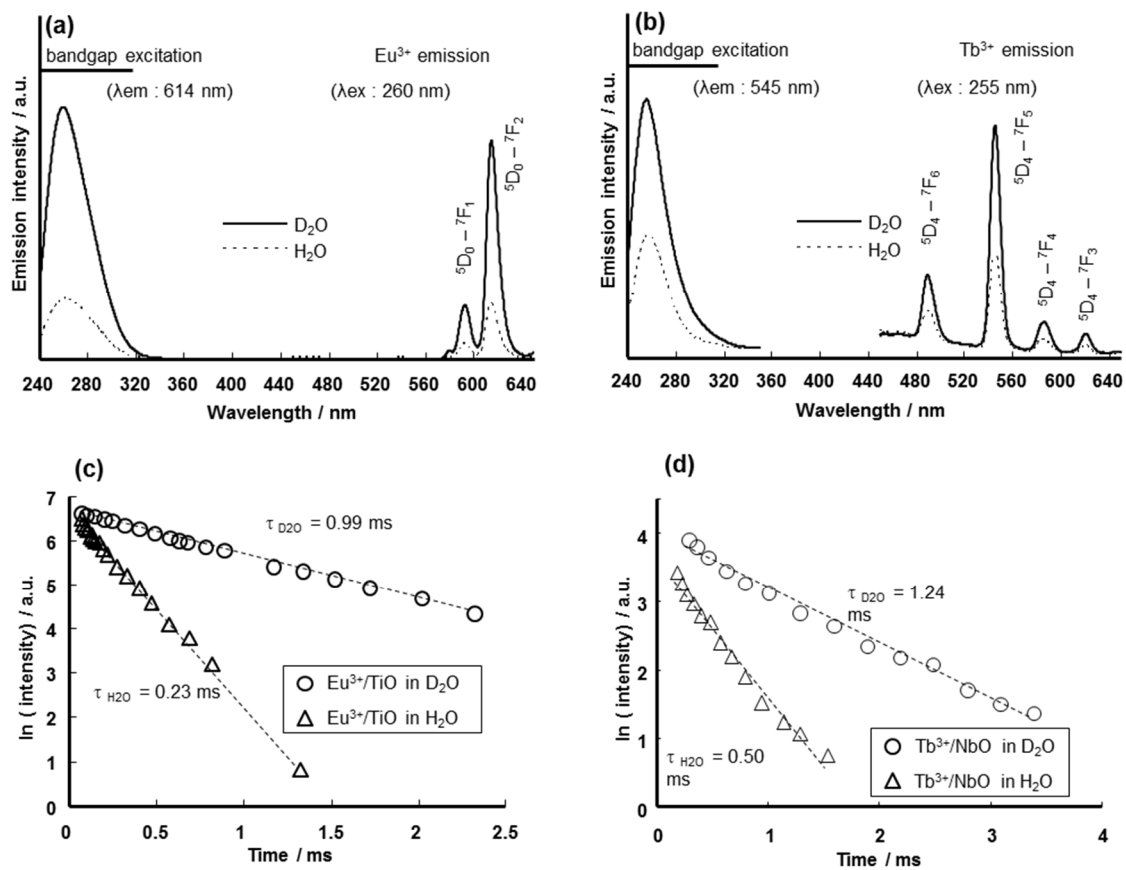


Figure 2-3. Photoluminescence spectra of the Eu³⁺/TiO (a) and Tb³⁺/NbO (b) in H₂O and D₂O. Time-resolved emission of the Eu³⁺/TiO and Tb³⁺/NbO are shown in (c) and (d) respectively.

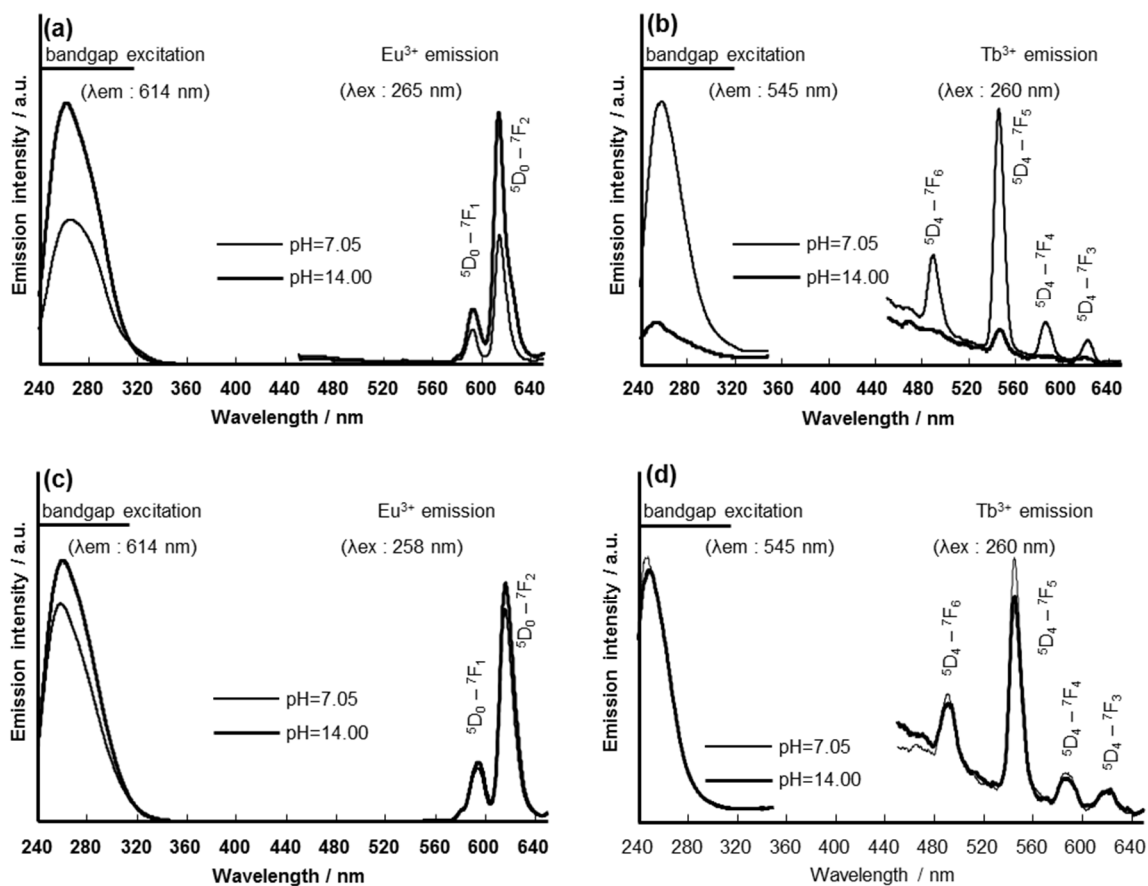


Figure 2-4. pH Dependences of emission intensities of Eu³⁺/TiO (a), Tb³⁺/NbO (b), Gd_{1.4}Eu_{0.6}Ti₃O₁₀ (GETiO) (c), and La_{0.7}Tb_{0.3}Ta₂O₇ (LTTaO) (d).

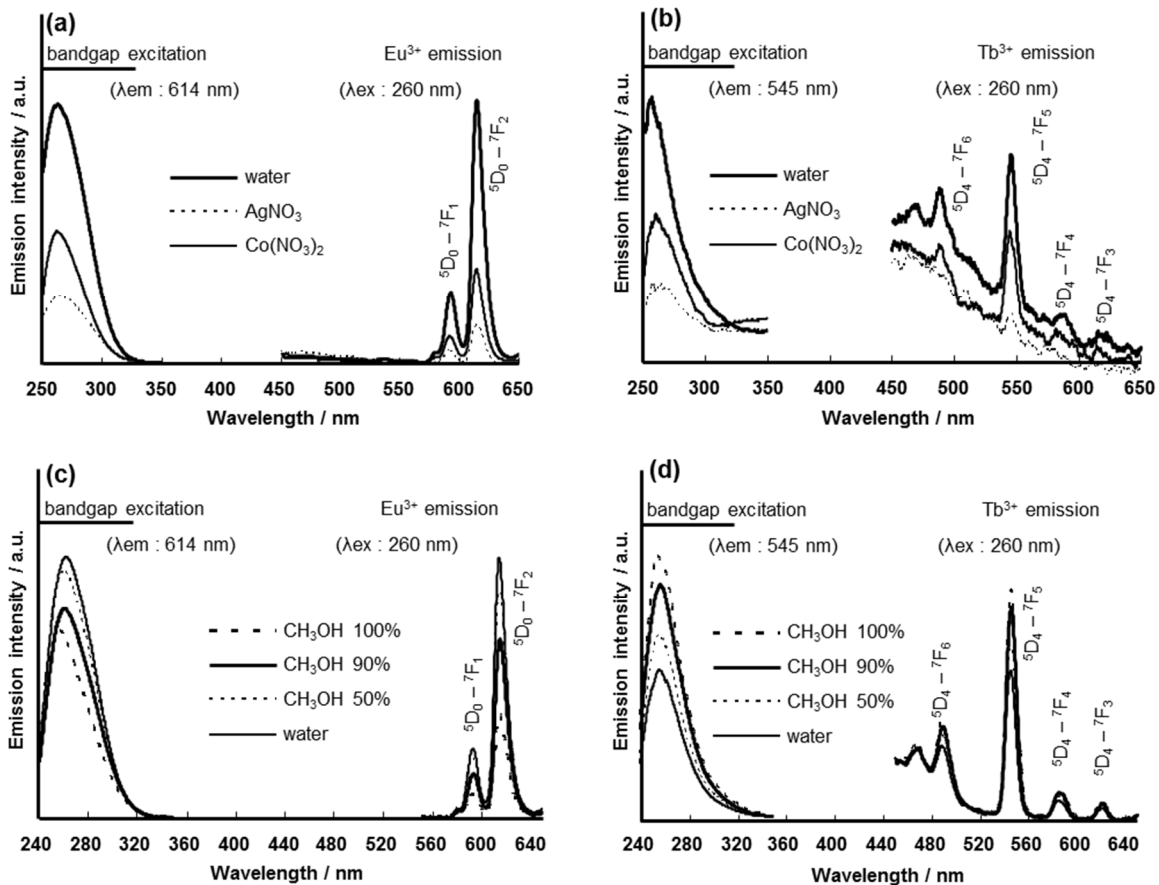


Figure 2-5. Photoluminescence spectra of the Eu³⁺/TiO (a and c) and Tb³⁺/NbO (b and d) in Ag⁺ and Co²⁺ solutions (a and b), and CH₃OH (c and d) solutions.

Table 2-1. Quantity of Exchange of the Ln³⁺ Ions of Solvents

Solvent	Eu ³⁺ /ppm	Tb ³⁺ /ppm
H ⁺	0	0.037
Co ²⁺	0	0
Ag ⁺	0	0.002

CHAPTER-III

Mass Production of Titanium (IV) Oxide Nanosheets by a Soft, Solution Process

overview

We succeeded in preparing titanium oxide nanosheets using a solution process under mild conditions. Concentrated nanosheet solutions were easily obtained by the addition of sodium dodecyl sulfate during the preparation of the layered oxide precursors. Our results indicate that titanium oxide nanosheets can be mass produced by a low-cost process, which is very important for their practical use. A drastic and specific enhancement of the photoluminescence of Eu^{3+} by energy transfer from the nanosheets occurred in the solution state, leading to a possibility of the trace analysis of Eu^{3+} .

3-1. Introduction

Nanosheets with two-dimensional structures having thickness of few nanometers possess very unique physical¹⁻³ and chemical properties.⁴⁻⁹ Some layered materials consisting of nanosheets (host layers) and intercalated molecules or cations also exhibit interesting properties owing to the interface between the nanosheets and the intercalated materials.¹⁰⁻¹³ Thus, nanosheets and their related materials are promising materials in science and practical use.

Titanium dioxide (TiO_2) has multiple unique properties. It acts as a photocatalyst for water splitting and decomposition of organic compounds under irradiation.¹⁵⁻¹⁶ It is an important substrate for dye-sensitized solar cells (Gratzel cell) and shows photoinduced super hydrophilicity.¹⁶⁻¹⁸ Moreover, layered titanium oxides act as a positive electrode in Li cells, where Li^+ intercalates into the titanium oxide interlayers.¹⁹

Titanium oxide nanosheets are the starting material for the preparation of new layered materials, where functional molecules or cations are intercalated between the titanium oxide host layers (i.e., nanosheets). They also exhibit unique photoluminescence (PL) properties^{10,11,20} based on the energy transfer from the titanium oxide host layers to lanthanide cations. In general, titanium oxide nanosheets have been prepared by the exfoliation of layered oxides with host layers and intercalated alkaline cations by multistep processing. For example, titanium oxide layered ceramics intercalated with Cs⁺ was prepared at high temperatures (>800 °C) and was protonated by acid leaching, followed by exfoliation to nanosheets in aqueous solutions.^{4,7} Thus, the preparation of titanium oxide nanosheets requires many steps that involve high-temperature processes. The concentration of the nanosheets is limited to $\sim 10^{-3}$ M (i.e., they are relatively dilute).

Recently, some solution methods for the preparation of titanium oxide layered materials under mild conditions (i.e., at room temperature) have been developed.²¹⁻²⁴ However, the exfoliation of the layered materials into nanosheets during solution processing is difficult. Imai et al. have reported the synthesis of titanium oxide nanodots by solution processing at room temperature.²⁴

In this paper, we demonstrate a novel, easy, and rapid solution method for the preparation of titanium oxide nanosheets under mild conditions, where concentrated nanosheet solutions (10^{-2} M) are obtained by the addition of sodium dodecyl sulfate (SDS) during precursor preparation. This approach represents a new mass-production technique for titanium oxide nanosheets necessary for their practical use. In addition, the specific enhancement of PL of Eu³⁺ by energy transfer from the nanosheets in a solution and a possibility of its trace analysis are presented.

3.2 Experimental

We synthesized titanium oxide nanosheet precursors by mixing aqueous solutions of $(\text{NH}_4)_2[\text{TiO}(\text{C}_2\text{O}_4)_2]$, KOH, and SDS (for DS nanosheets) as follows. Solutions of $(\text{NH}_4)_2[\text{TiO}(\text{C}_2\text{O}_4)_2]$, (0.13 M), KOH (2 M), and SDS (0.13 M) were prepared with distilled water. $(\text{NH}_4)_2[\text{TiO}(\text{C}_2\text{O}_4)_2]$, (20 mL), KOH (10 mL), and SDS (20 mL) were mixed in a 100 cm³ vessel to precipitate the nanosheet precursor and were stirred for 1 day at a temperature between room temperature and 80°C. After the reaction, the precipitates obtained were centrifuged (3000 rpm, 20 min), washed with distilled water and ethanol, and dried at room temperature under vacuum.

The exfoliation of the deposits ($\text{K}_{1.1}\text{H}_{0.9}\text{Ti}_2\text{O}_5 \cdot 2.6\text{H}_2\text{O}$) was performed as follows. The powdered material ($\text{K}_{1.1}\text{H}_{0.9}\text{Ti}_2\text{O}_5 \cdot 2.6\text{H}_2\text{O}$, 0.1 g) was mixed with a TBAOH aqueous solution (0.1 M, 100 mL) to exfoliate the host layers under slow stirring conditions for 1 day. The suspensions were subsequently centrifuged (3000 rpm, 10 min), and the supernatants were used as nanosheet solutions.

The crystal structure was analyzed using XRD patterns (Rigaku RINT-2500VHF, equipped with a Cu K α radiation source). The thickness of the exfoliated nanosheets was confirmed by AFM (Digital Instruments Nanoscope V, tapping mode) measurements; the samples for the AFM observations were prepared by spin coating of the diluted nanosheet solution onto mica substrates. The samples were dried under pure N₂ at room temperature. For TEM (Hitachi, HF-2000, 200 kV) observations, one drop of the aqueous nanosheet suspension was deposited onto a holey carbon film. XPS (Thermo Scientific, Sigma Probe) was used to analyze the layered oxides and nanosheets. A monochromatized X-ray source (Al K α , $h\nu = 1486.6$ eV) was used for the XPS measurements. For these measurements, a Pt substrate (in nanosheet/Pt film) was used

to determine the Fermi level. Raman spectroscopy was performed using a micro-Raman spectrometer (Jasco NRS-3100) with a 532 nm excitation source at room temperature. The concentration of the nanosheets in the solution was analyzed by an inductively coupled plasma spectrometer (Seiko Instruments, SPS7800), where the nanosheets were dissolved in the nanosheets were dissolved in concentrated HCl before measurements. UV–vis absorption spectra were obtained using a Jasco V-550 spectrometer. Thermogravimetric–differential thermal analysis curves for the layered oxides were obtained by thermal analysis (Seiko TG/DTA).

Photoluminescence spectra were analyzed with a Jasco FP-6500 spectrofluorometer equipped with a 150 W Xe lamp. Photoluminescence spectra of sample solutions ($\text{Eu}(\text{NO}_3)_3$, or nanosheet solutions, etc.) were prepared and placed in a square quartz cell.

3.3 Results and Discussion

Figure 3-1a shows a schematic illustration of the solution processes developed in this study to prepare titanium oxide nanosheets. The nanosheet precursors, i.e., layered oxides, were prepared in solutions with and without SDS. The deposited layered oxides were sufficiently washed with water so that DS^- anions scarcely existed in the samples, as stated below. Figure 3-1b shows X-ray diffraction (XRD) patterns of the prepared layered oxides. Both compositions of the layered oxides were $\text{K}_x\text{H}_{2-x}\text{Ti}_2\text{O}_5 \cdot n\text{H}_2\text{O}$ as stated below, and (200) diffractions were observed, independent of the presence of SDS during the synthesis process, as shown in Figure 3-1b. Figure 3-2 shows Raman spectra of both samples. These spectra also confirm the formation of the above layered oxide. Figure 3-1c shows high-resolution transmission electron microscopy (HR-TEM) images. Some clear layered structures were observed. Their basal spacings were ~ 0.95 nm, in agreement with those calculated from the XRD analyses (0.96 nm). According to

the X-ray photoelectron spectroscopy (XPS) analyses of the layered samples, the S/Ti ratio (in the case of SDS addition) was less than ~ 0.1 , indicating that the concentration of DS⁻ ions in the interlayers was very low. On the other hand, the K/Ti atomic ratios were 0.5–0.6 according to the XPS analysis, indicating that K⁺ ions existed in the interlayers of the layered oxide ($x = 1.1$). (As a matter of course, the K/Ti ratio was less than ~ 0.1 in the case of exfoliated nanosheets.) Some water molecules existed in the interlayers ($n = 2.6$) together with H⁺ ions (as H₃O⁺), according to thermal analysis, as shown in Figure 3-3. In general, DS⁻ ions intercalate into interlayers during solution processing,²⁵⁻²⁶ but they did not intercalate in the present case. The presence of DS⁻ ions in the reaction mixture brings about the formation of small titanium oxide nanosheets, and this resulted in concentrated nanosheet solutions because very small sized nanosheets are easily suspended in the aqueous solution, as will be discussed in a subsequent section. The DS⁻ ions will interact with TiO(C₂O₄)²⁻ complex ions and somewhat suppress the crystallization of the layered oxides during the solution process, leading to the formation of small sized nanosheets.

The layered oxides were exfoliated in tetrabutylammonium hydroxide (TBAOH) aqueous solutions, and nanosheet solutions were obtained by centrifugation at 3000 rpm to separate the deposits. The saturated concentrations of the titanium oxide nanosheets were about 10^{-2} and 10^{-4} M in the presence and absence of SDS during the preparation of the layered oxide precursors, respectively. Thus, SDS addition during layered precursor preparation resulted in a concentrated solution of nanosheets. Figure 3-4a shows Tyndall phenomena of both nanosheet solutions. Light scattering based on the concentrated nanosheets was observed in the case of the nanosheet solution obtained from the layered precursor prepared in the presence of SDS. Consequently, the approach using SDS during the preparation of the precursor, represents a new mass-production technique for titanium oxide nanosheets necessary for their practical use, as shown in Figure 3-5 .

In the present paper, the nanosheets exfoliated from precursors prepared in solutions with and without SDS are denoted as DS nanosheets and no-DS nanosheets, respectively. An atomic force microscopy (AFM) image of the no-DS nanosheets on a mica support is shown in Figure 3-4b. The thicknesses of the nanosheets ranged from 0.6 to 1.1 nm (which correspond to single and double nanosheets). Figure 3-4c shows a TEM image and selected-area electron diffraction (SAED) pattern of the no-DS nanosheets. The lateral sizes of the nanosheets were in range from 10 to 50 nm. The SAED pattern and unit cell (Figure 3-4c) indicate that the nanosheets consist of Ti_2O_5 with (001) faces. Figure 3-4 d shows HR-TEM images of the DS nanosheets. The lateral sizes were on the order of few nanometers, and the thicknesses ranged from 0.5 to 1.2 nm, as shown in Figure 3-6. Thus, the lateral size of the DS nanosheets is very small. Figure 3-4e shows a schematic illustration of the crystal structure of a single nanosheets. According to the XPS analysis, the nanosheets contain only Ti^{4+} , as shown in Figure 3-7 . Consequently, the nanosheets exist as $\text{Ti}_2\text{O}_5^{2-}$ ions in the solution.

Figure 3-8 a shows the effect of the presence of the $\text{Ti}_2\text{O}_5^{2-}$ nanosheets on the PL spectra of Eu^{3+} ions in the solution. The measurements were conducted in the suspension (solution) state. The emission and excitation spectra were measured at 275 nm excitation and 614 nm detection wavelengths, respectively. The emission peaks at 593 and 614 nm were assigned to the $^5\text{D}_0 \rightarrow ^7\text{F}_1$ magnetic dipole transition and the $^5\text{D}_0 \rightarrow ^7\text{F}_2$ forced electric dipole transition, respectively, of Eu^{3+} in the solution. The emission intensity of Eu^{3+} remarkably increased after nanosheet addition. As a matter of course, an intense red emission was observed for the Eu^{3+} solution with the nanosheets—but not for the solution without the nanosheets—under irradiation by a UV lamp, as shown in Figure 3-8 b. On the other hand, the emission intensities were very weak for Eu^{3+} solutions without the nanosheets and with P25 TiO_2 catalysts (size: 20 nm), where the emission

peaks were scarcely observed in the present conditions as shown in Figure 3-8 a. The excitation spectra of the solutions with the $\text{Ti}_2\text{O}_5^{2-}$ nanosheets were in agreement with the absorption spectrum of the nanosheet solution, where the onset wavelength was ~ 320 nm (The onset wavelength is shorter than that of bulk TiO_2 (400 nm) because of the quantum size effect.). Consequently, these results indicate that, during the excitation of the $\text{Ti}_2\text{O}_5^{2-}$ nanosheets under irradiation with light with an energy greater than the bandgap, energy transfer occurs from the $\text{Ti}_2\text{O}_5^{2-}$ nanosheets to the adsorbed Eu^{3+} , leading to the observed intense emission. In contrast, the energy transfer scarcely occurred in the case of P25 particles. This study represents the first report of such an energy-transfer emission in the solution state.

This energy transfer for the emission is characteristic in the combination of Eu^{3+} and the titanium oxide nanosheet, because the emissions of all the lanthanide ions were never promoted by the addition of the titanium oxide nanosheets. That is, the present specific emission of Eu^{3+} by the addition of the titanium nanosheets is available for a trace analysis of Eu^{3+} in the solutions contained many other lanthanide and/or other metal cations. Figure 3-8 c shows the emission spectra of Eu^{3+} ($10^{-8}\sim 10^{-5}$ M) in the solutions with 10^{-5} M nanosheets and its intensity as a function of Eu^{3+} concentration. The Eu^{3+} emission was observed even at 10^{-8} M, when the solutions contain the nanosheets. The straight line between the emission intensity and the dilute concentration of Eu^{3+} suggests that this method is useful for specific and trace quantitative analysis.

In the case of Eu^{3+} emission, the emissions due to magnetic dipole transitions are insensitive to site symmetry, whereas those due to electric dipole transitions are largely dependent on the site symmetry, i.e., inversion symmetry. If the Eu^{3+} site has no inversion symmetry, the electric dipole emission is strong, and the magnetic dipole transition becomes

relatively weak. On the other hand, if the Eu^{3+} site possesses inversion symmetry, the electric dipole emission is weak, and the magnetic dipole transition becomes relatively stronger. Hence, the $I_{614\text{nm}}(^5\text{D}_0-^7\text{F}_2)/I_{593\text{nm}}(^5\text{D}_0-^7\text{F}_1)$ emission intensity ratio is commonly used as a measure of the Eu^{3+} site symmetry.¹⁰ The ratio in the case of the Eu^{3+} solution with the nanosheets was ~ 4.4 and was larger than that of the Eu^{3+} solution without the nanosheets (0.4) (although the emission was very weak), suggesting that the site symmetry at Eu^{3+} is destructed in the solution with the nanosheets. In the present case, the Eu^{3+} site will correspond to the surrounding water field. The destruction of the symmetry of the Eu^{3+} site occurs because of the adsorption of Eu^{3+} onto the nanosheets in the solution. The present PL model of the Eu^{3+} adsorbed at a titanium oxide nanosheet is illustrated in Figure 3-8 d and Figure 3-8 e shows that a model for the energy transfer leading to photoluminescence in the $\text{Ti}_2\text{O}_5^{2-}$ nanosheet system.

3.4. Conclusion

We successfully obtained titanium oxide ($\text{Ti}_2\text{O}_5^{2-}$) nanosheets by exfoliating layered oxide precursors prepared by a solution process under mild conditions (i.e., room temperature ~ 80 °C). The concentrated nanosheet solutions were easily obtained when the layered oxide precursors were prepared in the presence of SDS, suggesting that the mass production of titanium oxide nanosheets by a low-cost process, which is important for the practical use of these nanosheets, is feasible. The drastic and specific enhancement of Eu^{3+} emission by energy transfer from the $\text{Ti}_2\text{O}_5^{2-}$ nanosheets occurred in the solution state. To the best of our knowledge, this study represents the first report of energy-transfer PL in an aqueous solution. The remarkable and specific enhancement of the emission by the energy transfer was very useful for a trace analysis of Eu^{3+} .

References

- (1) A.K.Geim, K. S. Novoselov, *Nat. Mater.*, 2007, 6, 183.
- (2) C. Lee, X. Wei, J. W. Kysar, J. Hone, *Science.*, 2008, 321, 385.
- (3) A. A. Balandin, S. Ghosh, W. Bao, I. Calizo, D. Teweldebrhan, F. Miao, C. N. Lau, *Nano Lett.*, 2008, 8, 902.
- (4) (a) T. Sasaki, M. Watanabe, H. Hashizume, H. Yamada, H. Nakazawa, *J. Am. Chem. Soc.*, 1996, 118, 8329. (b) T. Sasaki, M. Watanabe, *J. Am. Chem. Soc.*, 1998, 120, 4682.
- (5) F. Geng, R. Ma, A. Nakamura, K. Akatsuka, Y. Ebina, Y. Yamauchi, N. Miyamoto, Y. Tateyama, T. Sasaki, *Nat. Commun.*, 2013, 4, 1632.
- (6) (a) R. E. Schaak, T. E. Mallouk, *Chem. Mater.*, 2000, 12,2513.
(b) R. E. Schaak, T. E. Mallouk, T. E. *Chem. Mater.*, 2000, 12, 3427.
- (7) R. Abe, K. Shinohara, A. Tanaka, M. Hara, J. N. Kondo, K. Domen, *Chem. Mater.*, 2005, 17, 2487.
- (8) R. Abe, K. Shinohara, A. Tanaka, M. Hara, J. N. Kondo, K. Domen, *J. Mater. Res.*, 1998, 13, 861.
- (9) J. Wang, S. Yin, T. Sato, *Mater. Sci. Eng. B* 2006, 126, 53.
- (10) S. Ida, C. Ogata, M. Eguchi, W. J. Youngblood, T. E. Mallouk, Y. Matsumoto, *J. Am. Chem. Soc.*, 2008, 130, 7052.
- (11) (a) Ida, S.; Ogata, C.; Matsumoto, Y. *J. Phys. Chem. C* 2009, 113, 1896.
(b) S. Ida, C. Ogata, D. Shiga, K. Izawa, K. Ikeue, Y. Matsumoto, *Angew. Chem. Int. Ed.*, 2008, 47, 2480.
- (12) T. Sato, Y. Yamamoto, Y. Fujishiro, S. Uchida, *J. Chem. Soc. Faraday. Trans.*, 1996, 92, 5089.

- (13) L. Zhang, Q. Zhang, J. Li, *Adv. Funct. mater.* 2007, 17, 1958.
- (14) M. C. Tsai, J. C. Chang, H. S. Sheu, H. T. Chiu, C. Y. Lee, *Chem. Mater.*, 2009, 21, 499.
- (15) A. Fujishima, K. Honda, *Nature.*, 1972, 238, 37.
- (16) A. Fujishima, T. N. Rao, D. A. Tryk, *J. Photochem. Photo-biol. C* 2000, 1, 1.
- (17) (a) B. O'Regan, M. Gratzel, *Nature*, 1991, 353, 737-740. (b) M. Gratzel, *Nature*, 2001, 414, 338.
- (18) O. Carp, C. L. Huisman, A. Reller, *Prog. Solid State Chem.*, 2004, 32, 33.
- (19) (a) S. Ding, J. S. Chen, D. Luan, F. Y. C. Boey, S. Madhavi, X. W. Lou, *Chem. Commun.*, 2011, 47, 5780. (b) J. S. Chen, X. W. Lou, *Electrochem. Commun.*, 2009, 11, 2332.
- (20) A. Funatsu, S. Ida, C. Ogata, Y. Matsumoto, *Bull. Chem. Soc. Jpn.*, 2011, 8, 867.
- (21) T. Ohya, A. Nakayama, T. Ban, Y. Ohya, Y. Takahashi, *Chem. Mater.*, 2002, 14, 3082.
- (22) Y. Takezawa, H. Imai, *small.*, 2006, 3, 390.
- (23) B. Zhao, F. Chen, X. Gu, J. Zhang, *Chem. Asian. J.*, 2010, 5, 1546.
- (24) K. Nakamura, Y. Oaki, and H. Imai, *J. Am. Chem. Soc.*, 2013, 135, 4501.
- (25) S. Ida, D. Shiga, M. Koinuma, and Y. Matsumoto, *J. Am. Chem. Soc.*, 2008, 130, 14038-14039.
- (26) (a) T. Taniguchi, Y. Sonoda, M. Echikawa, Y. Watanabe, K. Hatakeyama, S. Ida, M. Koinuma, and Y. Matsumoto, *ACS Appl. Mater. Interfaces.*, 2012, 4, 1010-1015. (b) T. Taniguchi, M. Echikawa, Y. Naito, H. Tateishi, A. Funatsu, C. Ogata, Y. Komatsubara, N. Matsushita, M. Koinuma, and Y. Matsumoto, *J. Mater. Chem.*, 2012, 22, 20358.
- (27) C. E. Bamberger, G. M. Begun, and C. S. MacDOUGALL, *Appl. Spectros.*, 1990, 44, 30.
- (28) F. Maxim, P. Ferria, and P. M. Vilarinho, *J. Porous. Mater.*, 2011, 18, 37.
- (29) F. Maxim, P. Ferria, and P. M. Vilarinho, *J. Mater. Chem.*, 1997, 7, 777.

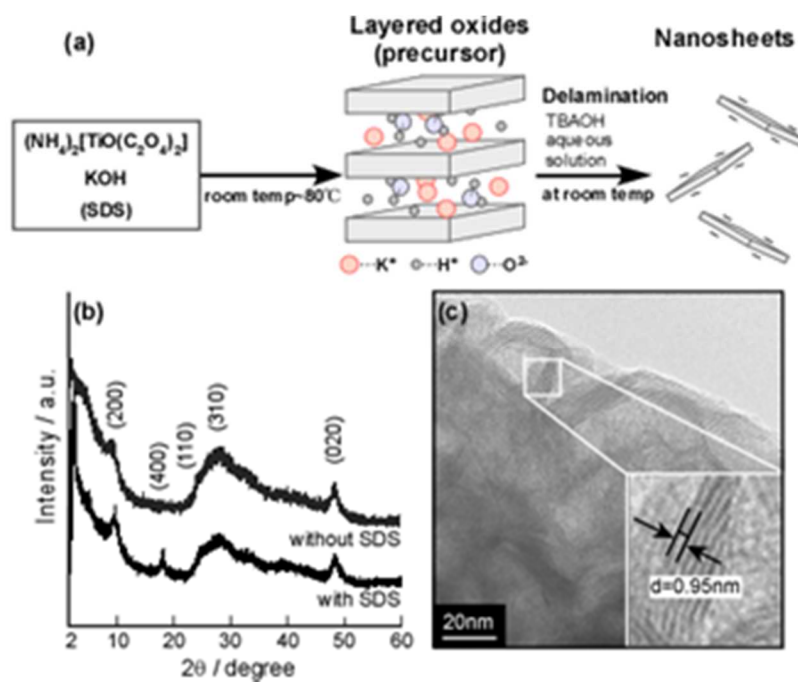


Figure 3-1. (a) Schematic illustration of the solution process developed for the production nanosheets, (b) XRD patterns of the layered oxides, and (c) HR-TEM image of the layered oxide as a nanosheet precursor.

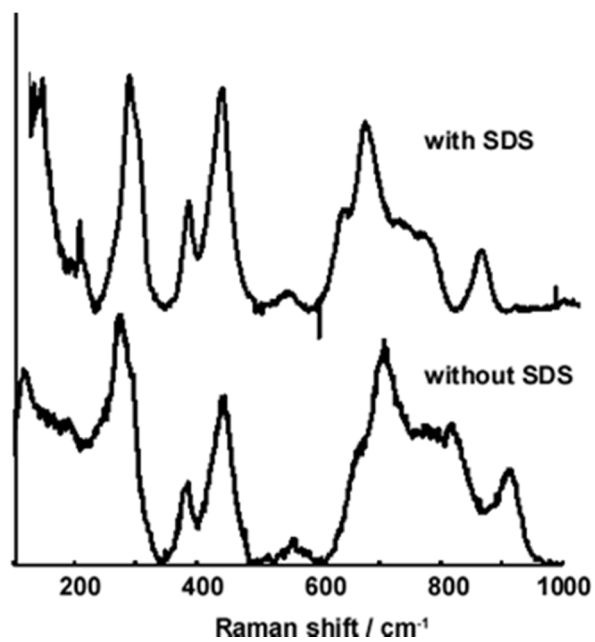


Figure 3-2. Raman spectra of the prepared layered titanium oxides. These spectra are in agreement with those of $\text{Na}_{2-x}\text{H}_x\text{Ti}_2\text{O}_5 \cdot 1.8\text{H}_2\text{O}$, $\text{K}_2\text{Ti}_2\text{O}_5$, and water-treated $\text{Cs}_2\text{Ti}_2\text{O}_5$.²⁷⁻²⁹

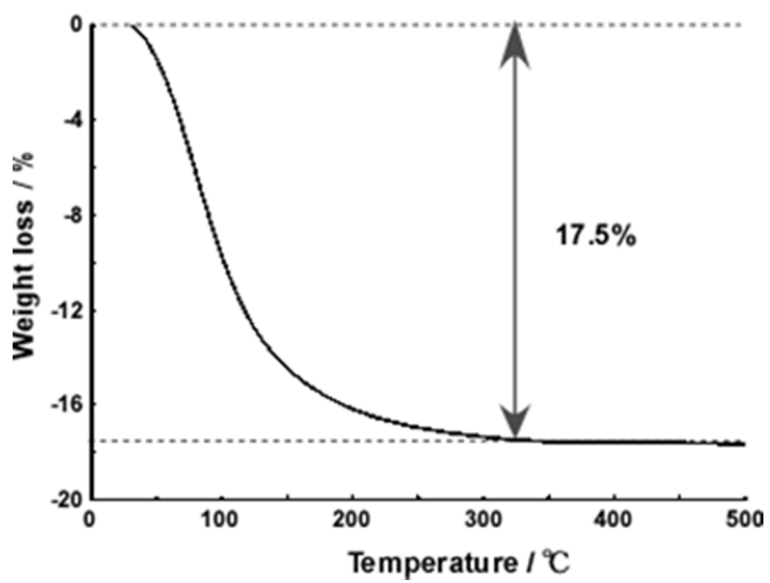


Figure 3-3. Thermal analysis (TG) results of the layered oxide. The mass loss of 17.5% at temperatures less than ~330 °C is due to the release of intercalated water.

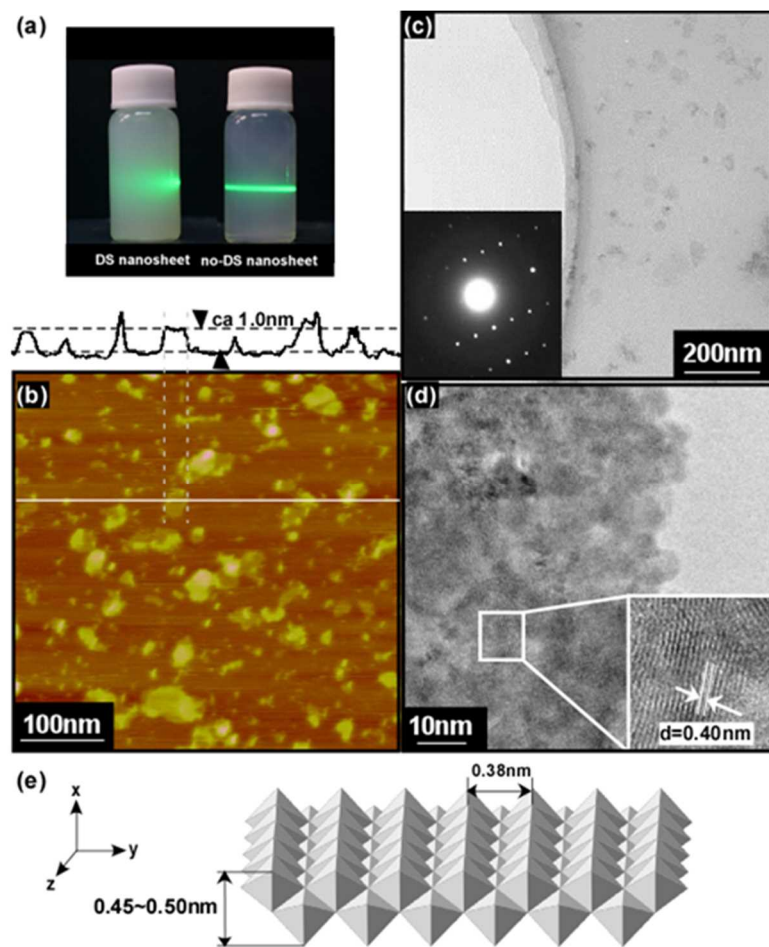


Figure 3-4. (a) Photograph of the Tyndall phenomena of nanosheet solutions, (b) AFM image of the no-DS nanosheets, (c) TEM image and SAED pattern of the no-DS nanosheets, (d) HR-TEM image of the DS nanosheets, and (e) crystal-structure model of a $\text{Ti}_2\text{O}_5^{2-}$ single nanosheet.



Figure 3-5. Photograph of the mass-product DS nanosheet solution (2L, $3.9 \times 10^{-3} \text{M}$).

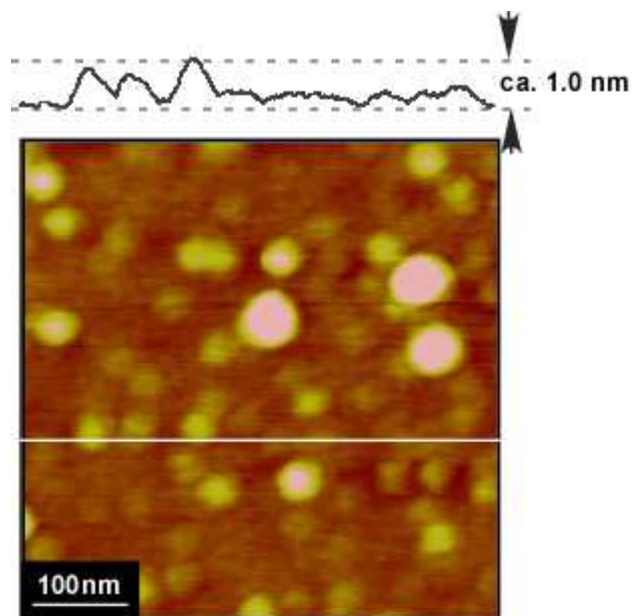


Figure 3-6. AFM image and depth profile of the DS nanosheets. Because of the nanosheets' small lateral sizes (few nanometers), they appear as particles (the limitation of the AFM tip with respect to lateral size is ~10–20 nm).

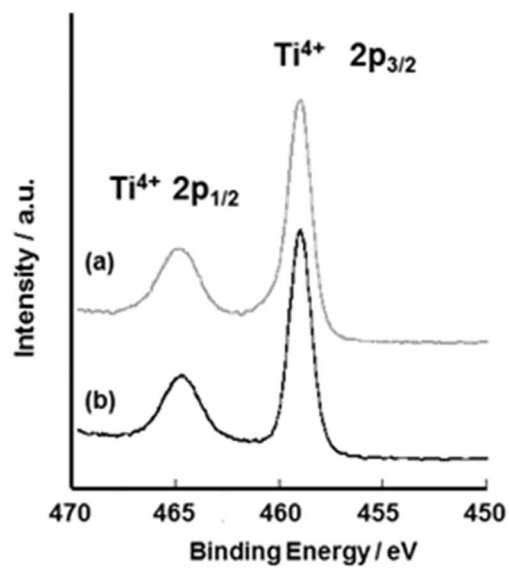


Figure 3-7. XPS spectra of Ti_{2p_{1/2}} and 2p_{3/2} for (a) layered oxide precursor and (b) nanosheets. All of Ti exist as Ti⁴⁺.

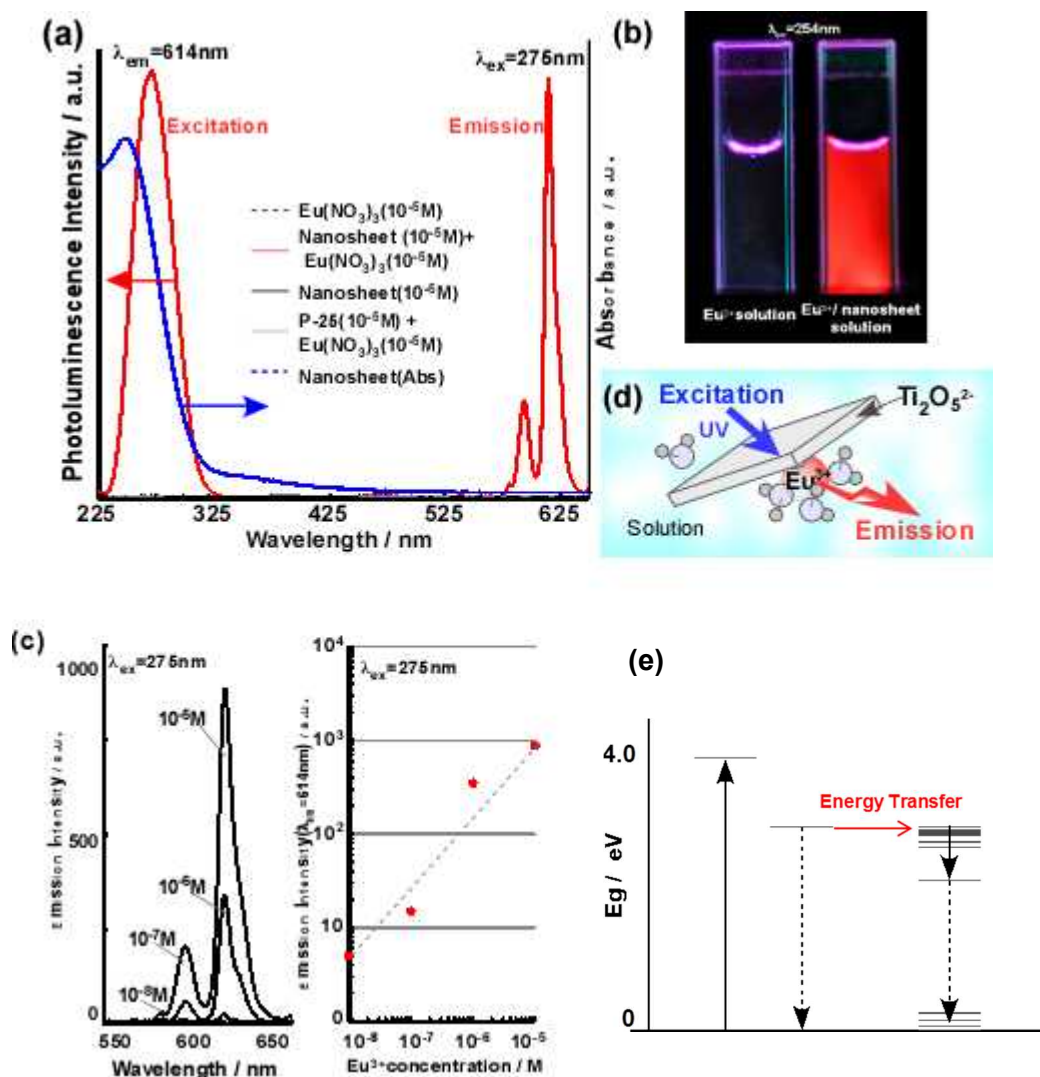


Figure 3-8. (a) Photoluminescence spectra of various solutions containing 10^{-5} M $\text{Eu}(\text{NO}_3)_3$ and UV-vis absorption spectra of the nanosheet solutions, (b) Photographs of the 10^{-5} M solutions of $\text{Eu}(\text{NO}_3)_3$ and $\text{Eu}(\text{NO}_3)_3 / \text{nanosheets} (10^{-5} \text{ M})$ under irradiation with a UV lamp (254 nm), (c) Emission spectra of Eu^{3+} (from 10^{-8} and 10^{-5} M) in the solutions with 10^{-5} M nanosheets and its intensity as a function of Eu^{3+} concentration, (d) Illustration of the mechanism of energy transfer from the nanosheets to the adsorbed Eu^{3+} , and (e) A model for the energy transfer leading to photoluminescence in the $\text{Ti}_2\text{O}_5^{2-}$ nanosheet system.

CHAPTER-IV

Nd³⁺-Doped Perovskite Nanosheets with Tailored NIR Luminescence

Overview

Metal-oxide nanosheets with near-infrared (NIR) luminescent properties were synthesized for the first time by the exfoliation of $\text{KLa}_{1-x}\text{Nd}_x\text{Nb}_2\text{O}_7$ layered perovskite. The colloidal nanosheets demonstrate a luminescent band at 1060 nm as a result of the ${}^4\text{F}_{3/2}\text{--}{}^4\text{I}_{11/2}$ (Nd^{3+}) transition upon excitation at 808 nm. Organic-surface modification greatly enhanced the luminescence while maintaining a high colloidal stability.

4.1 Introduction

Nanosheets have been extensively investigated for the fabrication of ultrathin devices. For example, graphene is a potential nanosheet material^{1,2} that can replace Si devices in the near future. In addition, metal oxide nanosheets³⁻¹⁴, which are prepared by exfoliating layered metal oxides, have attracted considerable interest as building blocks for the fabrication of advanced devices using soft-chemical strategies^{11,14}. Their properties are largely tunable by doping heterometallic ions into the structure, thus affording a variety of unique features, including optical⁴⁻¹¹, catalytic¹², electrical¹³, and dielectric¹⁴ properties.

Trivalent rare-earth (Re) ion-doped nanosheets with well-characterized 4f–4f luminescence are potential next-generation nanophosphors^{4-5,7-9}. For example, layer-by-layer assembly of nanosheets enables the fabrication of optically transparent films with improved luminescent properties¹¹. As another application, luminescent nanosheets are highly suitable materials for bioanalytical devices. Owing to the extremely ultrathin nature of nanosheets (ca. 1 nm in thickness), their luminescence can be strongly influenced by surface adsorbed components, such

as ions and molecules, enabling potential applications as bioimaging probes and bioanalytical sensors that are sensitive to external fields and various stimuli¹⁵.

To date, luminescent nanosheets with blue⁵, green⁴, and red^{4,7-8} emissions have been synthesized; however, these nanosheets are often impractical for biochemical applications as they require ultraviolet light excitation, which may damage the target system or produce interfering background luminescence. In fact, much effort has been devoted to finding novel organic and inorganic bioprobes that can be excited by an 800–1700-nm light source in the range of the biological window¹⁶⁻¹⁸.

In the present study, we have for the first time developed Nd³⁺-activated nanosheets with NIR luminescence. We demonstrated that Nd³⁺-doped LaNb₂O₇ perovskite nanosheets with a 1.75-nm thickness yielded (⁴F_{3/2}–⁴I_{11/2}) Nd³⁺ luminescence via excitation at 808 nm and further succeeded in enhancing their luminescent properties as well as their colloidal stability via organic surface modification.

4.2 Experimental

Materials.

Layered KLa_{1-x}Nd_xNb₂O₇ were prepared as follows. The synthesis of KLa_{1-x}Nd_xNb₂O₇ (x= 0.025, 0.05, 0.1, 0.2, 0.3) was carried out using a conventional solid-state procedure. The starting material was a stoichiometric mixture of K₂CO₃, La₂O₃, Nd₂O₃, and Nb₂O₅. (K₂CO₃ was 99.5 % purity purchased from Wako Chemicals Co., Ltd. La₂O₃ was 98.0 % purity purchased from Wako Chemicals Co., Ltd. Nd₂O₃ was 99.9 % purity purchased from Wako Chemicals Co., Ltd. Nb₂O₅ was 99.9 % purity purchased from Wako Chemicals Co., Ltd.)The mixture was heated at 900°C for 4h and 1100°C for 40h.

Protonation was carried out by stirring 1g of $\text{KLa}_{1-x}\text{Nd}_x\text{Nb}_2\text{O}_7$ powder in 300mL of 1M aqueous HCl solution for 7days at room temperature. (K_2CO_3 , was 99.9 % purity purchased from Wako Chemicals Co., Ltd.) After reaction, obtained solid product was centrifuged and washed with deionized Milli-Q water.

Exfoliation.

The exfoliation of the $\text{HLa}_x\text{Nd}_{1-x}\text{Nb}_2\text{O}_7$ was carried out as follows. The protonated powder (1.0 g) was exfoliated in 8 times tetrabutylammoniumhydroxide (TBAOH) (300 mL) for 7days. (TBAOH solution was 40.0 % purity purchased from Kanto Chemicals Co., Ltd.) The subsequent centrifugation of the solution under 3000 rpm for 30 min yielded colloidal suspension of $\text{La}_{1-x}\text{Nd}_x\text{Nb}_2\text{O}_7$ nanosheets.

Preparation of nanosheets by surface modification.

The preparation of the $\text{La}_{1-x}\text{Nd}_x\text{Nb}_2\text{O}_7$ -nanosheets solution was by surface modification carried out as follows. The $\text{La}_{1-x}\text{Nd}_x\text{Nb}_2\text{O}_7$ -nanosheets solution (5ml), 1mg/ml 3-aminopropyltriethoxysilane (0.05ml) and 10mg/ml polyacrylic acid (0.05ml). (3-aminopropyltriethoxysilane was from Shinetsu Chemicals Co., Ltd. polyacrylic acid, was from Wako Chemicals Co., Ltd.)

4.3 Results and Discussion

The synthesized $\text{KLa}_x\text{Nd}_{1-x}\text{Nb}_2\text{O}_7$ contained single-layered perovskite blocks (see Figure 4-1(a)) with intercalated K^+ . The A and B sites in the perovskite blocks can accommodate Ln (La^{3+} and Nd^{3+}) and Nb cations, respectively. Figure 4-1(b) and (c) show XRD patterns of

KLaNb_2O_7 and $\text{KLa}_{1-x}\text{Nd}_x\text{Nb}_2\text{O}_7$ ($X = 0.30$, the maximum Nd^{3+} doping concentration investigated in the present study). Both patterns correspond well to the KLaNb_2O_7 structure, indicating the successful substitution of Nd^{3+} for La^{3+} even at a very high concentration; this is mostly due to the similar ionic radii of these ions. The sharp peaks demonstrate the highly crystalline nature of the sample. SEM-EDX analysis of as-synthesized $\text{La}_{1-x}\text{Nd}_x\text{Nb}_2\text{O}_7$ -microplates confirmed that all the metallic elements were distributed uniformly in the products (see Figure 4-2).

The mechanism for the NIR luminescence of the Nd^{3+} ions is described as follows. First, an 808-nm photon excites Nd^{3+} ions to the $^4\text{F}_{5/2}$ level, after which they decay nonradiatively to the lower $^4\text{F}_{3/2}$ level to produce NIR emission with radiative transitions (see Figure 4-3(a)). Figure 4-3(b) shows the photoluminescence (PL) spectra of the starting material ($\text{KLa}_{1-x}\text{Nd}_x\text{Nb}_2\text{O}_7$) at various La/Nd ratios (Nd is 2.5%, 5%, 10%, 20%, and 30%) resulting from excitation at 808 nm. All samples yielded NIR luminescence as a result of the Nd^{3+} radiative transitions corresponding to $^4\text{F}_{3/2} \rightarrow ^4\text{I}_{9/2}$ (880nm), $^4\text{F}_{3/2} \rightarrow ^4\text{I}_{11/2}$ (1060nm), and $^4\text{F}_{3/2} \rightarrow ^4\text{I}_{13/2}$ (1350nm)^{6,19}. The sample with 2.5-mol% Nd^{3+} produced the strongest emission. The decrease in the emission intensity for the samples with higher concentrations of Nd^{3+} resulted from concentration quenching due to the cross-relaxation process accompanying the change in the relative band intensities. Because they had the highest emission intensity, the 2.5-mol% Nd^{3+} -doped samples were studied in the following investigations.

Intercalated K^+ ions were exchanged with protons by treatment with 1 M HCl. Protonation was carried out by stirring $\text{KLa}_{0.975}\text{Nd}_{0.025}\text{Nb}_2\text{O}_7$ powder in a 1 M aqueous HCl solution at room temperature. Figure 4-4 shows the XRD patterns of $\text{HLa}_{0.975}\text{Nd}_{0.025}\text{Nb}_2\text{O}_7$ as protonated layered oxides. The interlamellar distance decreases on proton exchange. Figure 4-5(a) shows PL spectra

for $\text{KLa}_{0.975}\text{Nd}_{0.025}\text{Nb}_2\text{O}_7$ and $\text{HLa}_{0.975}\text{Nd}_{0.025}\text{Nb}_2\text{O}_7$ resulting from excitation at 808 nm. The figure indicates that proton exchange decreases the PL intensity. In the cation exchange process, the proton is intercalated as an oxonium ion (H_3O^+). It is presumed that the high-energy OH vibration of the intercalated H_3O^+ is coupled with the Nd^{3+} energy levels. As a result, the rate of nonradiative transition increased significantly. Notably, we observed a decrease in the relative intensity of the high - energy stark component of the $^4\text{F}_{3/2}$ doublet to low-energy one, where they were observed at 1050 nm to 1070 nm, respectively. A decrease in the relative band intensity was also detected with an increase in the Nd^{3+} concentration (Figure 4-3). These results revealed that the relative intensity of these peaks is strongly influenced.

We performed exfoliation of the host layer to prepare single layer nanosheets. Figure 4-5(b) shows typical atomic force microscopy (AFM) images of $\text{La}_{0.975}\text{Nd}_{0.025}\text{Nb}_2\text{O}_7$ nanosheets obtained by exfoliation of $\text{HLa}_{0.975}\text{Nd}_{0.025}\text{Nb}_2\text{O}_7$ with a tetrabutylammonium hydroxide aqueous solution. Cross-sectional analysis of the AFM data demonstrated that the thickness of the nanosheets was approximately 1.75 nm, a value that corresponded well to that of the perovskite layers in the initial materials. SAED patterns from single nanosheets displayed well-defined square spots, indicating that each sheet is a single crystal(see Figure 4-6(c)). Figure 4-6(d) shows PL spectra for the aqueous colloidal $\text{La}_{0.975}\text{Nd}_{0.025}\text{Nb}_2\text{O}_7$ nanosheets. The colloids yielded the main Nd^{3+} transitions at $^4\text{F}_{3/2}-^4\text{I}_{11/2}$ (1060 nm), though the emission was weakly detected. Unlike those of the protonated layered structure, the OH ligands in the perovskite nanosheet layers were directly coordinated with metal ions. These surface hydroxyl groups should more strongly couple with the Nd^{3+} energy levels than those from intercalated H_3O^+ in the protonated layered structure, resulting in remarkable quenching effects. Furthermore, considering the single layer thickness, all the luminescent Nd^{3+} centers might interact with OH such that surface quenching occurs more

in the nanosheets than in conventional nanoparticles. In other words, this indicates that the luminescence properties of the nanosheets would be highly sensitive to changes in the surface environment, such as surface modifications.

Next, we attempted to enhance the luminescent properties by organic surface passivation. Among the potential modification techniques, we employed silylation²⁰⁻²³, whereby the surface hydroxyl groups were treated with an aminopropylsilane reagent (3-aminopropyltriethoxysilane, APTES). Surface modification was performed by a one-pot process in which a $\text{La}_{0.975}\text{Nd}_{0.025}\text{Nb}_2\text{O}_7$ nanosheet solution was mixed with an aqueous solution of APTES. As expected, the emission intensity of the nanosheets increased approximately threefold (Figure 4-7(a)) by reaction with APTES for 5 min. The result suggested that Si–O bonding rapidly replaced surface H–O bonding, which suppressed the nonradiative transition rate. Note that the surface modification particularly increased the high-energy Stark component of the $^4\text{F}_{3/2}$ doublet at 1060 nm rather than low-energy one, leading to luminescent spectra similar to that of protonated layered material, which further indicated that the Si–O bonding decreased the number of OH species coordinated directly to the surface.

Although we observed improved luminescence at the initial reaction stage, the luminescence was quenched after the reaction continued for one day. Along with the luminescence quenching, we observed an aggregation of the nanosheets resulting in the sedimentation of the products. The aggregation was likely caused either by the lateral polymerization of APTES on the nanosheets, leading to (nanosheet)–O–Si–O–Si–O–(nanosheet) bonding, or by the attachment of the APTES NH_3^+ groups to the surface of the negatively charged unmodified nanosheets (see Figure 4-6 (c), Figure 4-7, and 4-8).

We discovered that polyacrylic acid (PAA) was an efficient secondary additive, providing

high colloidal and luminescent stability. For instance, on adding a mixture of APTES and PAA to the nanosheet colloidal solution, no aggregation was observed. This is because the carboxyl groups of PAA can attach to the positively charged APTES-modified nanosheets and thereby prevent aggregation. In addition to improved colloidal stability, luminescent properties were enhanced by adding PAA. This demonstrates that APTES can be grafted onto the nanosheets to form an initial organic layer, and PAA can then be adsorbed onto APTES. The emission intensity of the nanosheets finally increased six-fold after the reaction for more than one day, which is remarkably higher than that of the surface modified nanoparticulate phosphors²⁴⁻²⁷. For example²⁶, it is reported that a two-fold enhancement of YVO₄:Eu PL was achieved by coating with SiO₂, while a 1.1-fold²⁶ improvement in the PL properties of (Y,Gd)BO₄:Eu³⁺ was observed by forming SiO₂ or SiO₂-Al₂O₃ shells. We also note that APTES-modification of multi-layered KLa_{0.975}Nd_{0.025}Nb₂O₇ nanoplates gave no enhancement of PL intensity (Figure 4-9). As all the luminescent Nd³⁺ centers of nanosheets located at the surface region due to the extremely thin thickness, surface states could be much strongly emphasized in nanosheets rather than in nanoparticles. As a result, nanosheets could offer such unusually strong enhancement in luminescent properties by the surface modification. These results also suggest that the nanosheets can be smart NIR sensors where luminescent intensity is able to be switched depending on surface species and reactions.

4.4. Conclusion

In this study, we successfully synthesized NIR luminescent metal oxide nanosheets for the first time by the exfoliation of KLa_{1-x}Nd_xNb₂O₇ layered perovskite. The colloidal nanosheets afford 1060-nm luminescence resulting from ⁴F_{3/2}-⁴I_{11/2} (Nd³⁺) transitions upon excitation at 808

nm. Surface modification of nanosheets by APTES and PAA resulted in six-fold enhanced luminescent intensity while maintaining a high colloidal stability. Our study demonstrated that Nd³⁺-doped nanosheets exhibit NIR luminescent properties with their large tunability depending on surface states, which will lead to the development of smart bioimaging probes and bioanalytical sensors.

References

- (1) A. K. Geim, K. S. Novoselov, *Nat. Mater.*, 2007, 6, 183.
- (2) Y. Matsumoto, M. Koinuma, S. Ida, S. Hayami, T. Taniguchi, K. Hatakeyama, H. Tateishi, Y. Watanabe, and S. Amano, *J. Phys. Chem.C* 2011, 115, 19280.
- (3) J. Gopalakrishnan, V. Bhat, *Mater. Res. Bull.*, 1978, 22, 413.
- (4) S. Ida, C. Ogata, M. Eguchi, W. Justin Youngblood, T. Mallouk, and Y. Matsumoto, *J. Am. Chem. Soc.*, 2008, 130, 7052.
- (5) S. Ida, C. Ogata, U. Unal, K. Izawa, T. Inoue, O. Altuntasoglu, and Y. Matsumoto, *J. Am. Chem., Soc.* 2007, 129, 8956.
- (6) S. Ida, Y. Sonoda, and Y. Matsumoto, *J. Ceramic. Process. Res.*, 2011, 12, s17.
- (7) T. Ozawa, K. Fukuda, K. Akatsuka, Y. Ebina, T. Sasaki, K. Kurashima, and K. Kosuda, *J. Phys. Chem.C* 2008, 5, 1312.
- (8) T. Ozawa, K. Fukuda, K. Akatsuka, Y. Ebina, and T. Sasaki, *Chem. Meter.*, 2007, 19, 6575.
- (9) K-H Lee, B-I Lee, J-H You and S-H Byeon, *Chem. Commun.*, 2010, 1461.
- (10) T. Sasaki, M. Watanabe, *J. Phys. Chem. B* 1997, 101, 10159.
- (11) M. Osada, T. Sasaki, K. Ono, Y. Kotani, S. Ueda, and K. Kobayashi, *ACS Nano.*, 2011, 5, 6871.
- (12) Y. Ebina, T. Sasaki, M. Harada, and M. Watanabe, *Chem. Mater.*, 2002, 14, 4390.
- (13) B-W. Li, M. Osada, T. C. Ozawa, Y. Ebina, K. Akatsuka, R. Ma, H. Funakubo, and T. Sasaki, *ACS Nano.*, 2010, 4, 6673.
- (14) M. Osada, and T. Sasaki, *J. Appl. Ceram. Technol.*, 2012, 9, 29.
- (15) S. Ida, C. Ogata, D. Shiga, K. Izawa, K. Ikeue, and Y. Matsumoto, *Angew. Chem. Int. Ed.*, 2008, 47, 2480.

- (16) K. Soga, K. Tokuzen, K. Tsuji, T. Yamano, H. Hyodo, and H. Kishimoto, *Eur. J. Inorg. Chem.*, 2010, 2673.
- (17) R. R. Anderson, and J. A. Parrash, *J. Invest. Dermatol.*, 1981, 77, 13.
- (18) T. Taniguchi, K. Soga, K. Tokuzen, K. Tsujiuchi, T. Kidokoro, K. Tomita, K. Katsumata, N. Matsushita, and K. Okada, *J. Mater. Sci.*, 2012, 47, 2241.
- (19) V. Buissette, A. Huignard, T. Gacoin, J-P. Boilot, P. Aschehoug, and B. Viana, *Surface Science.*, 2008, 532-535, 444.
- (20) J. Y. Kim, H. Hiramatsu, and F. E. Osterloh, *J. Am. Chem. Soc.*, 2005, 127, 15556.
- (21) D. Boudinet, M. Benwadih, S. Altazin, J-M. Verilhac, E. D. Vito, C. Serbutoviez, G. Horowitz, and A. Facchetti, *J. Am. Chem. Soc.*, 2011, 133, 7052.
- (22) T. Yanagisawa, K. Kuroda, and C. Kato, *Reactivity of Solids.*, 1988, 5, 167.
- (23) Y. Ide, and M. Ogawa, *Chem. Commun.*, 2003, 1262.
- (24) S. Lechevallir, P. Hammer, J. M. Caiut, S. Mazeres, R. Mauricot, M. Verelst, H. Dexpert, S. J. Ribeiro, and J. D.-Ghys, *Langmuir.*, 2012, 28, 3962.
- (25) B. Y. Wu, H. F. Wang, J. T. Chen, and X. P. Yan, *J. Am. Chem. Soc.*, 2011, 133, 15556.
- (26) Y. Wang, W. Qin, J. Zhang, C. Cao, S. Lu, and X. Ren, *Optics. Commun.*, 2009, 282, 1148.
- (27) J. H. Seo, and S. H. Soho, *Mater. Lett.*, 2010, 64, 1264.

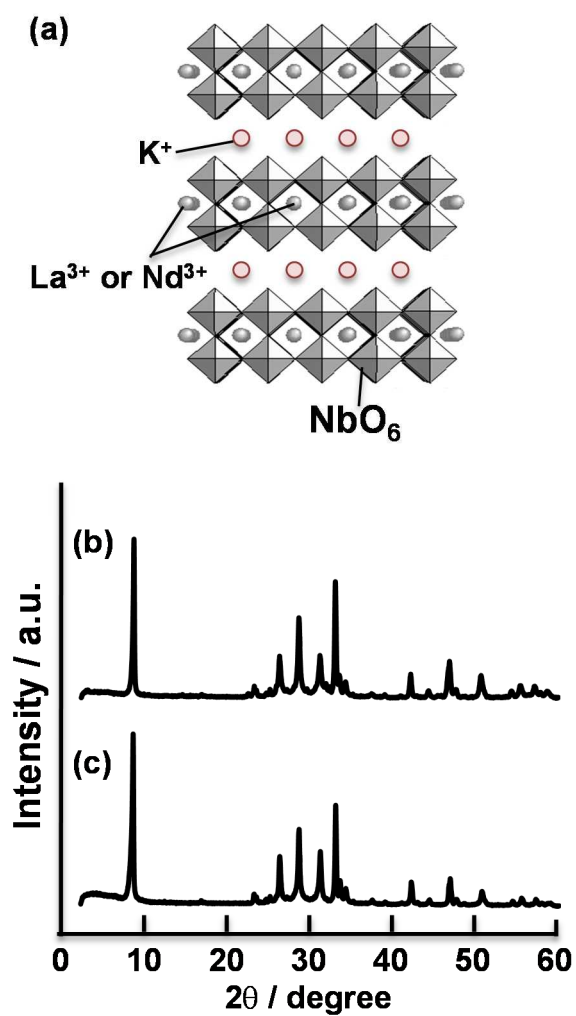


Figure 4-1 (a) structural model of layered $\text{KLa}_{1-x}\text{Nd}_x\text{Nb}_2\text{O}_7$, XRD pattern of layered (b) KLaNb_2O_7 , and (c) $\text{KLa}_{0.7}\text{Nd}_{0.3}\text{Nb}_2\text{O}_7$

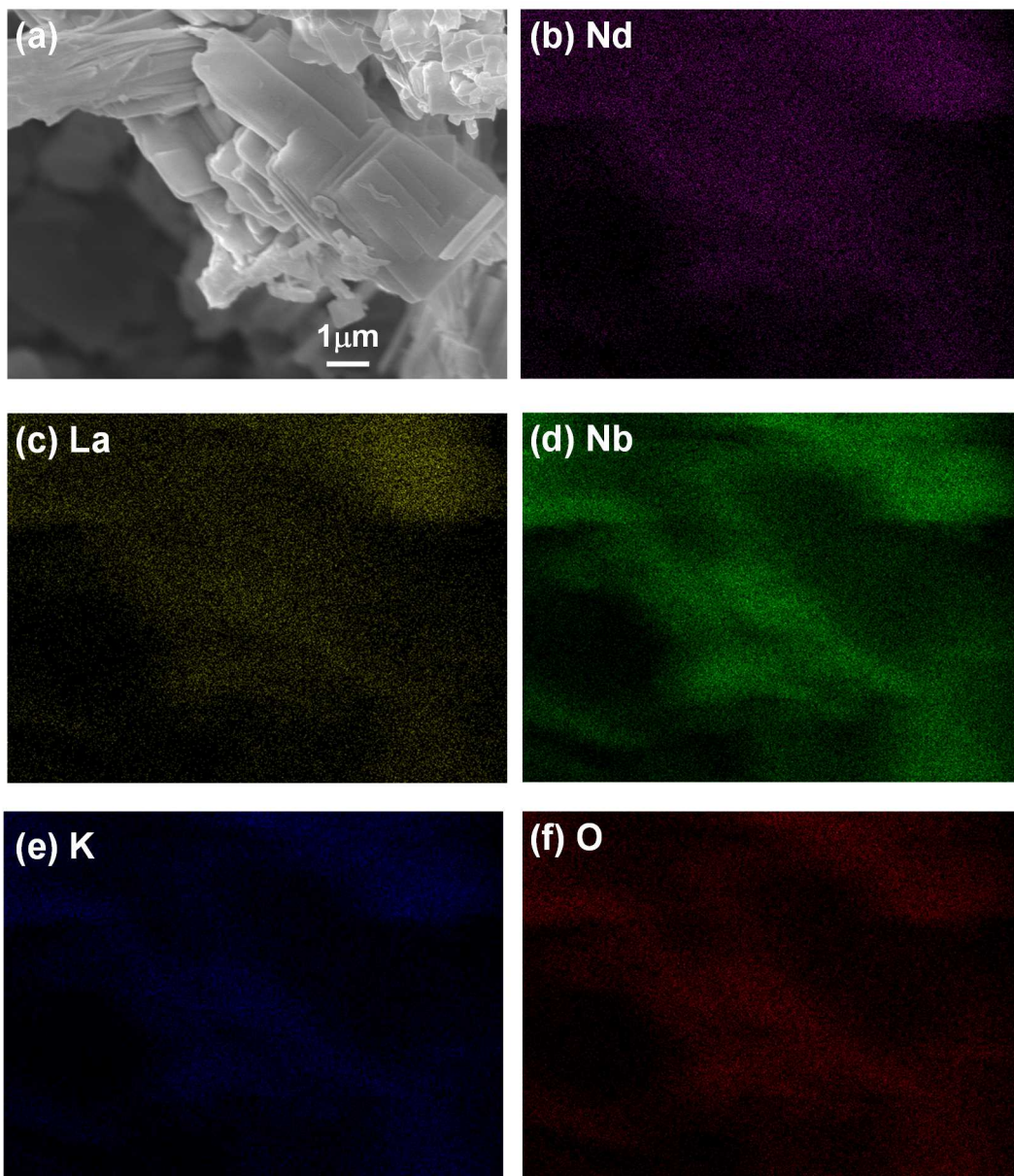


Figure 4-2. FE-SEM image and EDX analysis of the layered $\text{KLa}_{1-x}\text{Nd}_x\text{Nb}_2\text{O}_7$.

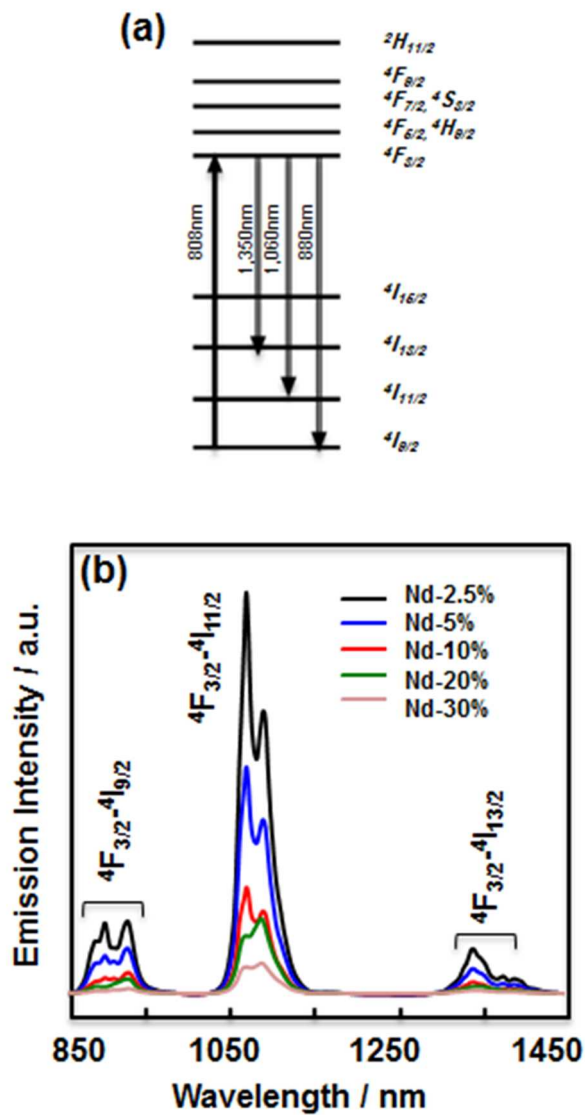


Figure 4-3. (a) Energy level diagram of Nd^{3+} . (b) PL spectra of starting material $(\text{KLa}_{1-x}\text{Nd}_x\text{Nb}_2\text{O}_7)$ at various La/Nd ratios (97.5/2.5: Nd-2.5%, 95/5: Nd-5%, 90/10: Nd-10%, 80/20: Nd-20%, 70/30: Nd-30%) (λ_{ex} :808nm).

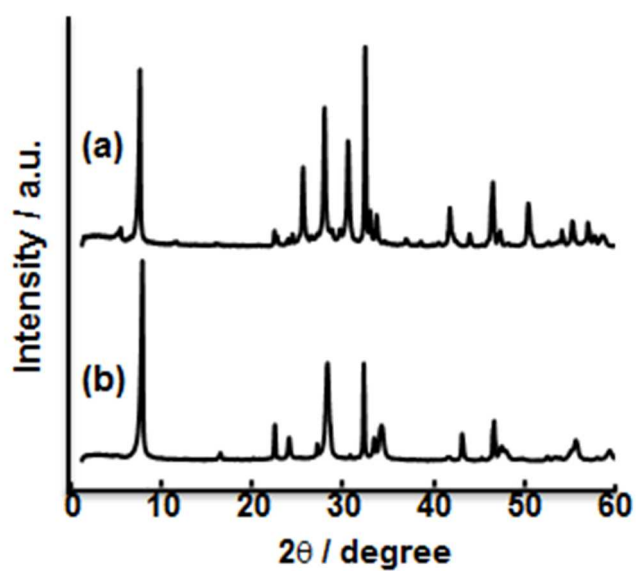


Figure 4-4. XRD patterns of the layered perovskite starting materials (a) $\text{KLa}_{0.975}\text{Nd}_{0.025}\text{Nb}_2\text{O}_7$ and (b) $\text{H La}_{0.975}\text{Nd}_{0.025}\text{Nb}_2\text{O}_7$.

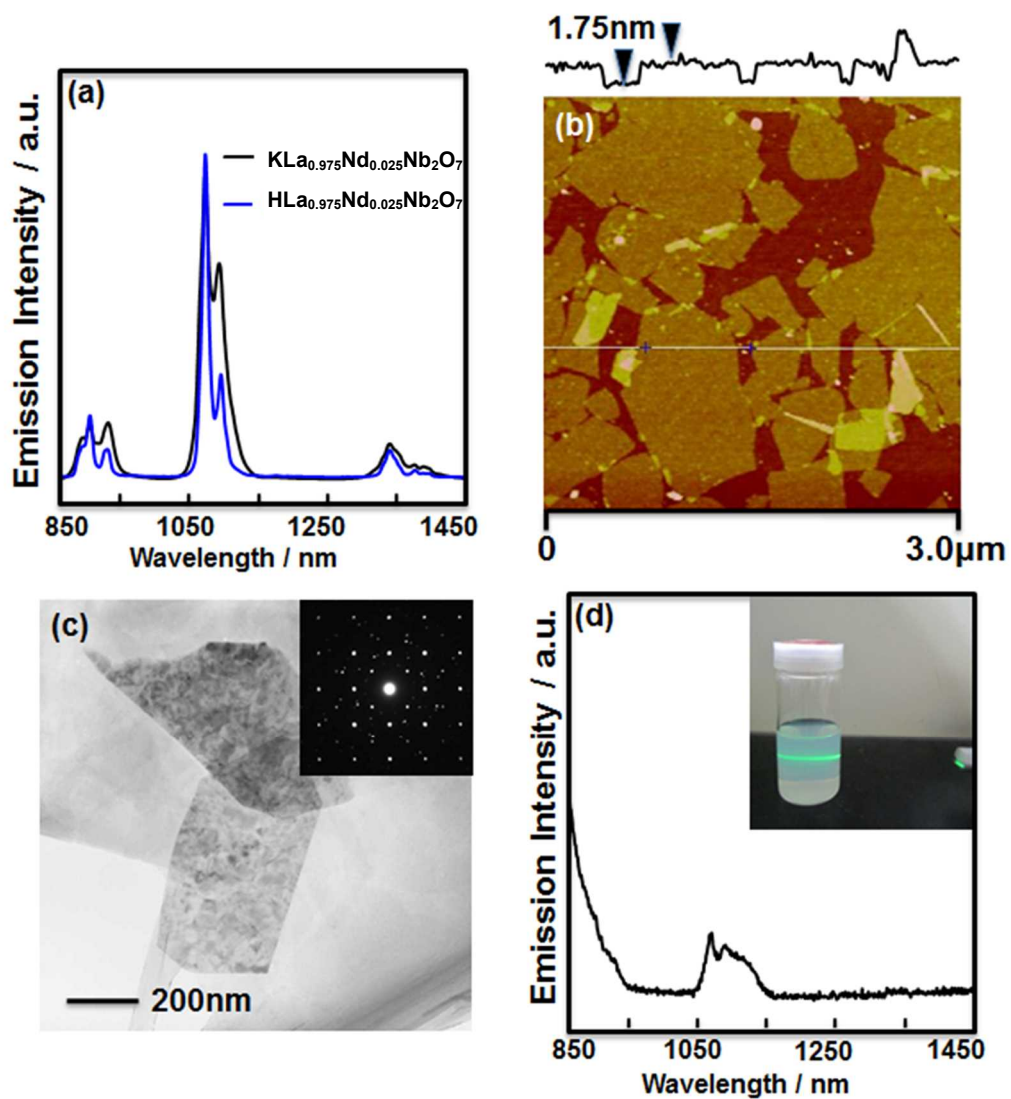


Figure 4-5. (a) PL spectra of $\text{KLa}_{0.975}\text{Nd}_{0.025}\text{Nb}_2\text{O}_7$ and $\text{HLa}_{0.975}\text{Nd}_{0.025}\text{Nb}_2\text{O}_7$ ($\lambda_{\text{ex}} : 808\text{nm}$). (b) AFM image of monolayer film of $\text{La}_{0.975}\text{Nd}_{0.025}\text{Nb}_2\text{O}_7$ -nanosheet. (c) TEM images of $\text{La}_{0.975}\text{Nd}_{0.025}\text{Nb}_2\text{O}_7$ nanosheet. (d) PL spectra of $\text{La}_{0.975}\text{Nd}_{0.025}\text{Nb}_2\text{O}_7$ -nanosheet solution ($\lambda_{\text{ex}} : 808\text{nm}$).

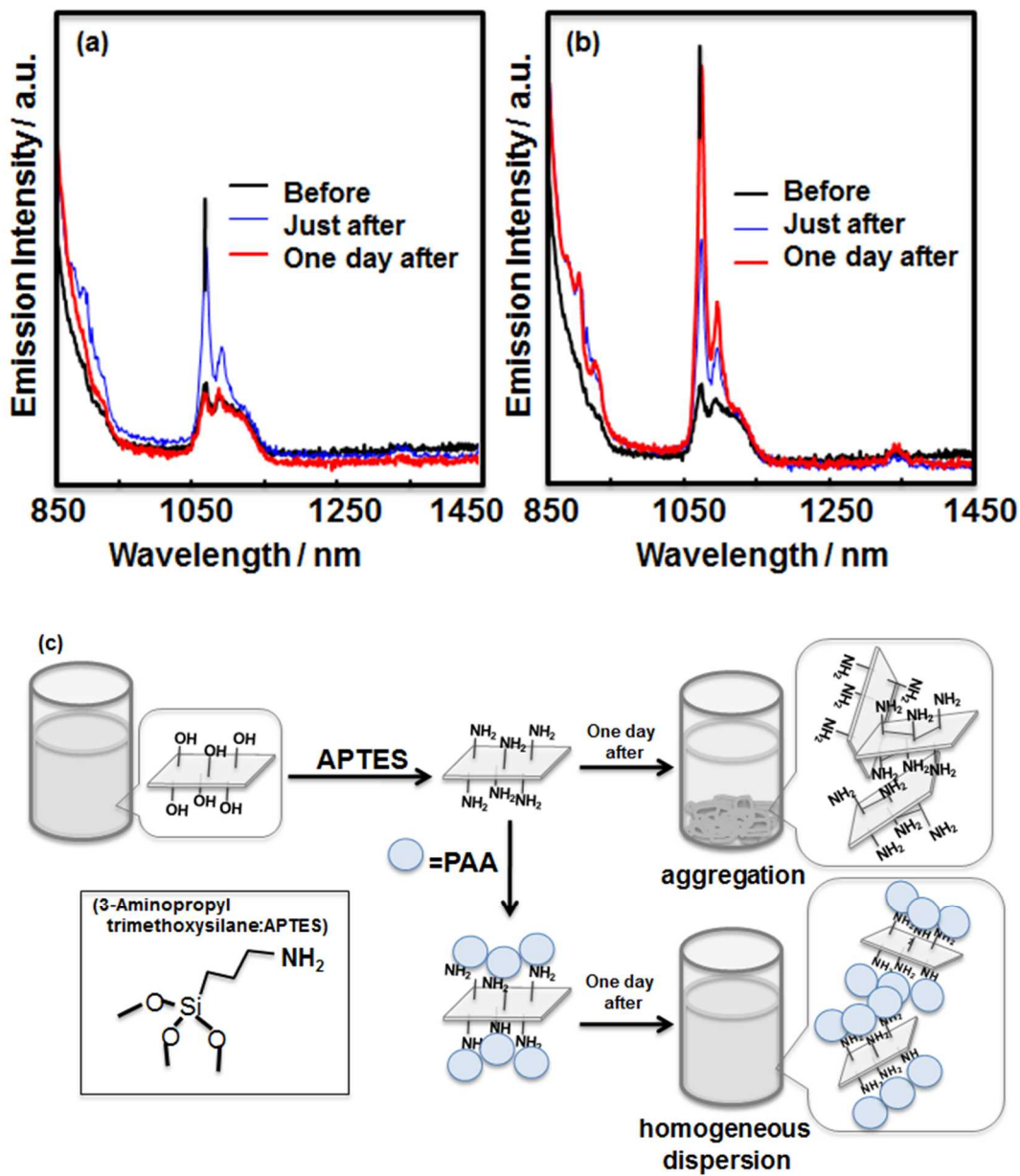


Figure 4-6. (a) PL spectra of K La_{0.975}Nd_{0.025}Nb₂O₇ and H La_{0.975}Nd_{0.025}Nb₂O₇ (λ_{ex} : 808nm). (b) AFM image of monolayer film of La_{0.975}Nd_{0.025}Nb₂O₇ nanosheet. (c) TEM images of La_{0.975}Nd_{0.025}Nb₂O₇ -nanosheet. (d) PL spectra of La_{0.975}Nd_{0.025}Nb₂O₇ nanosheet solution (λ_{ex} : 808nm).

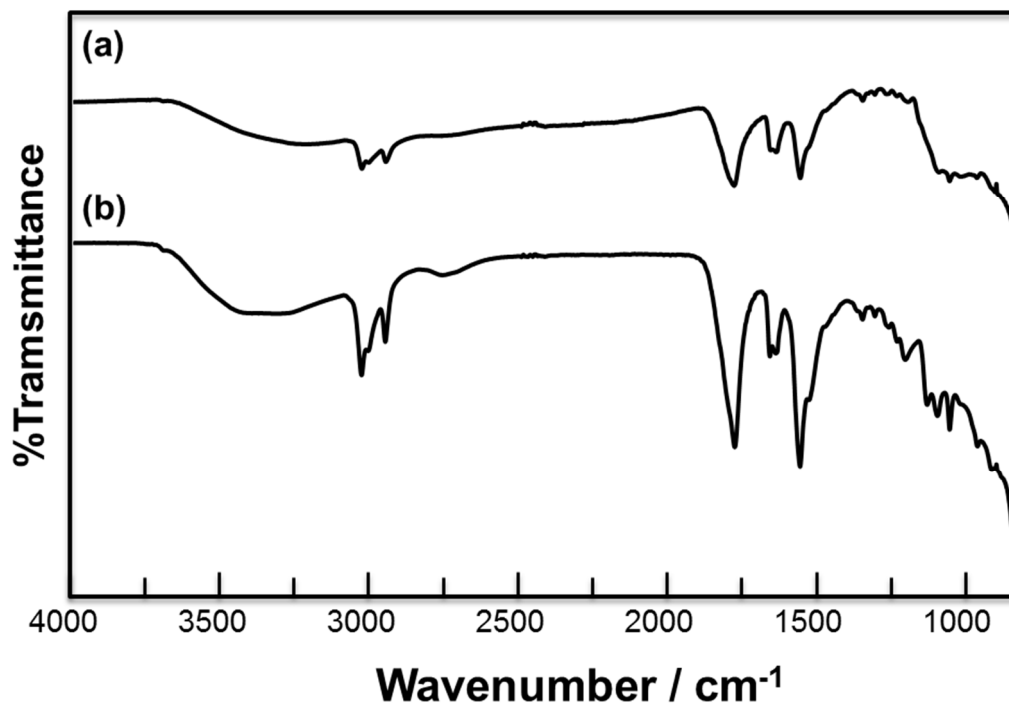


Figure 4-7. FT-IR spectra of the $\text{La}_{0.975}\text{Nd}_{0.025}\text{Nb}_2\text{O}_7$ nanosheet (a) as prepared and (b) nanosheets by surface modified APTES.

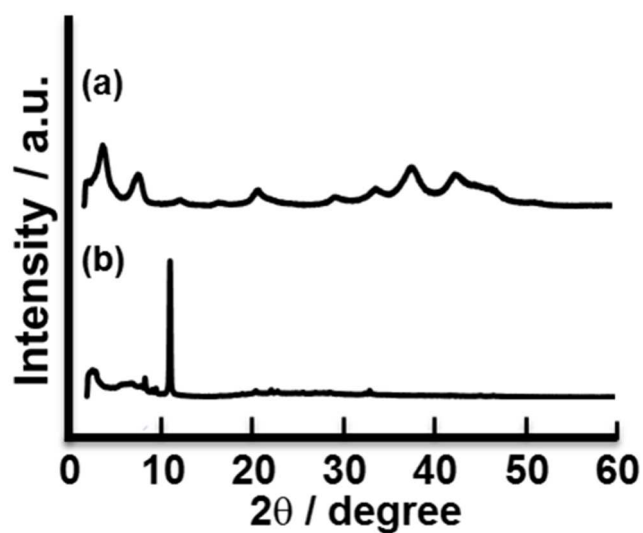


Figure 4-8. XRD patterns of the $\text{La}_{0.975}\text{Nd}_{0.025}\text{Nb}_2\text{O}_7$ -nanosheet (a) as prepared and (b) nanosheets by surface modified APTES.

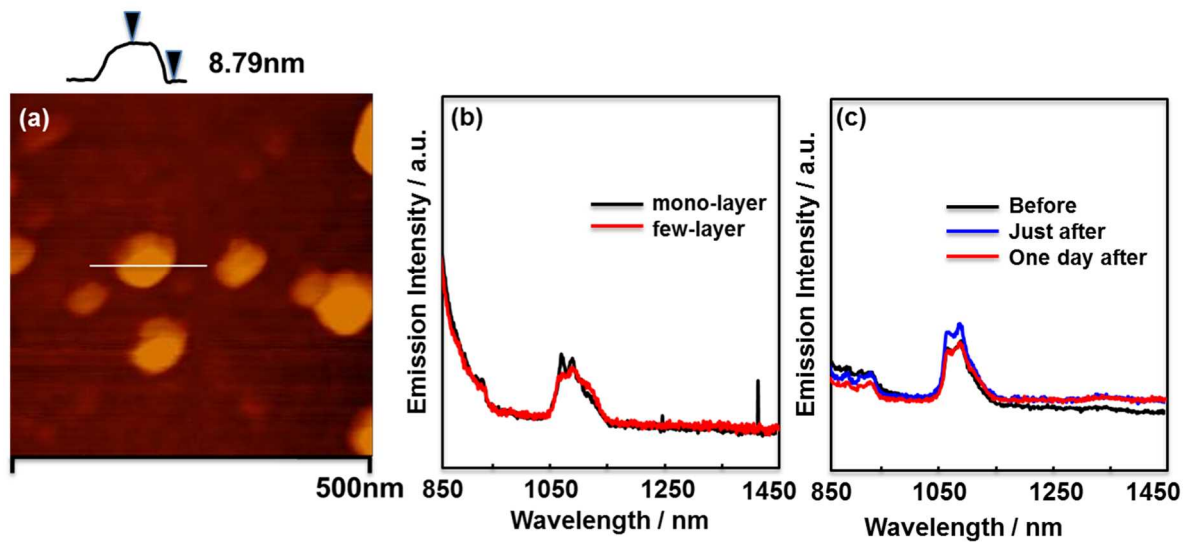


Figure 4-9. (a) AFM image of $\text{La}_{0.975}\text{Nd}_{0.025}\text{Nb}_2\text{O}_7$ -few layer nanoplate. (b) PL spectra of mono-layer and few-layered nanosheets (λ_{ex} : 808nm), (c) PL spectra of multi-layered nanoplates by surface modified APTES (λ_{ex} : 808nm)

CHAPTER-V

Immobilization of Trypsin on Graphene Oxide Nanosheets for Increased Proteolytic Stability

Overview

To increase the thermal and chemical stabilities of trypsin proteolysis activity, trypsin was immobilized on graphene oxide nanosheets (GONSs) by a one-step diimide-activated amidation. The trypsin-immobilized GONS (1.9 mg per mg-GONS) showed significantly higher thermal and chemical stabilities than the free form. After heat treatment at 50 °C for 6 h, the trypsin-GONS retained 80% of its initial activity, but free trypsin retained only 4% of its initial activity.

5.1 Introduction

In recent years, the immobilization of bioactive molecules on solid supports has given rise to a wide range of academic and industrial applications, e.g., immobilized enzyme reactors for proteomics.¹ Proteases are the predominant industrial enzymes, accounting for about 60% of total worldwide sales.² Immobilized enzymes are reusable and easily removed from the digestion medium. Several reports have demonstrated proteolytic performances using enzymes immobilized on various supports such as magnetic nanoparticles,³ nanodiamonds,⁴ mesoporous activated carbon,⁵ mesoporous silica,⁶ and glass beads.⁷

Immobilization methods can be divided into two classes: physical methods and chemical methods.⁸ Physical adsorption methods have the advantages of simplicity and low cost, but a major disadvantage is that the enzyme is easily desorbed from the support.⁹ In comparison, when the enzyme is firmly immobilized on the support by a covalent method, its stability toward

chemical denaturants and organic solvents can be enhanced.^{10,11} However, covalent methods are more complicated and expensive.

Graphene and graphene oxide (GO), carbon nanomaterials, have good potential for biological applications, because of their biological compatibility.^{12,13} Recently, GO nanosheets (GONSs) have attracted attention as potentially useful materials for bioapplications because of their unique properties such as planar morphology, chemically active surface area, and stability toward corrosive media.^{14,15} The surface of the GONS is covered with a variety of functional groups including carboxy, epoxy, and hydroxy groups, which may be easily activated for conjugation of biological molecules. Moreover, GONSs have high surface ratios ($2600\text{m}^2\text{ g}^{-1}$)¹⁶ and also high dispersibility in liquid media because of their oxidized, hydrophilic surfaces.

In this paper, we report a simple and natural method for the preparation of enzyme-immobilized GONSs by the diimideactivated amidation of GONS-bound carboxylic acids. Trypsin was used as a model enzyme for the investigation. In order to study the actual stabilization of immobilized trypsin, we also compared the thermal and chemical stabilities of the immobi immobilized trypsin with the free-trypsin stabilities under various conditions.

5.2 Experimental

Preparation of GO and GO nanosheets

Pure graphite powder (Wako Pure Chemical Industries Ltd., Osaka, Japan) (0.5 g) was oxidized by a modified Hummers' method¹⁷ in which NaNO_3 (0.5 g), H_2SO_4 (23 mL), and KMnO_4 (3 g) were mixed in an ice bath and H_2O_2 solution (30%, 3 mL) and H_2O (40 mL, distilled water) were then added at a high temperature (35-95 °C). The resulting mixture was washed several times with distilled water and then dried in an oven. The resulting GO was

suspended in distilled water (1.2 mg/mL), sonicated in an ultrasonic bath for 2 h, and centrifuged to remove any aggregated GO. Exfoliated GO was collected in a vial (nanosheet suspension).¹⁸

Preparation of trypsin-immobilized GO nanosheets

The method used for immobilization of trypsin on GONSs is shown in Scheme 1. Carboxylic acid groups on the surface of GO nanosheets (GONS) were activated using a carbodiimide [1-ethyl-3-(3-dimethylaminopropyl)-carbodiimide hydrochloride; EDC] and subsequently reacted with N-hydroxysuccinimide (NHS) to provide reactive sites for covalent attachment to trypsin.^{19,20} A GONS dispersion (5 mL, 500 $\mu\text{g mL}^{-1}$) and 5 mg of NHS were prepared in a 50mM MES buffer solution (pH 6). With ultrasonic assistance, 6 mg of EDC was added quickly, and the mixture was continually stirred at room temperature for 1 h. The dispersion was then centrifuged and rinsed thoroughly with MES buffer solution to remove excess EDC, NHS, and urea byproduct. The precipitate of the esterified GONS was re-dispersed in 1mL of MES buffer solution. Then enzyme (5 mg) was added and the mixture was stirred at 4 °C for 1 h. After immobilization, the pellet was washed with the MES buffer solution, and then with 1mL of glycine solution (1 M) to block unreacted epoxy groups. The supernatant solution was collected to measure the amount of immobilized trypsin; the immobilized amount was determined by measuring the residual concentration of the enzyme in the supernatant solution. Finally, the dispersion was centrifuged and rinsed thoroughly with MES buffer solution, and then resuspended in the buffer solution and stored at 4 °C. The dispersion obtained was used as the trypsin-GONS dispersion.

Assay of trypsin activity

The proteolytic activities of free trypsin and trypsin-GONS were determined by incubating 1 mL of diluted soluble sample (free trypsin solution or trypsin-GONS dispersion in phosphate buffer) with 1 mL of 1.5% casein solution and 1 mL of H₂O for 10 min at 37 °C. After incubation, 3 mL of 0.4 M trichloroacetic acid solution were added to stop the reaction immediately. The reaction mixture was allowed to stand for 15 min at room temperature and then filtered. Filtrate (1 mL) was mixed with 5 mL of 0.55 M Na₂CO₃ solution and 1 mL of 1 N Folin reagent. After thorough distribution, colorimetric cylinders were incubated for 30 min at 37 °C. The immobilization ability of the GONS for trypsin was evaluated by measuring the UV absorption of the supernatant trypsin solution after immobilization. The absorbance of the produced DL-tyrosine was detected at 660 nm. One unit (U) of enzyme activity was defined as the quantity of enzyme that releases 1.0 µg-tyrosine/min at pH 7.0 and 37 °C. All activity tests were performed at least in triplicate.

The relationship between the initial rate of reaction and casein concentration (0.2–2.0%) in 0.02 M phosphate buffered saline solution (pH 7.0) at 37 °C was determined. The Michaelis–Menten kinetic parameters (i.e., the Michaelis constant, K_m , and the maximum effective velocity, V_{max}) were calculated from Lineweaver–Burk double reciprocal plots:

$$1/V = 1/V_{max} + (K_m/V_{max}) \times 1/S$$

The thermal stability of the enzyme was determined by measuring the residual enzymatic activity after exposure at 5–50 °C for given time intervals of several hours. Ethanol solution was chosen as the enzyme denaturant. The enzyme was treated with ethanol solution with volume percentages ranging from 10% to 50% (v/v) at 37 °C for 30 min, and then the residual enzymatic activity was determined.

Characterization and Equipment.

Fourier-transform infrared (FT-IR) spectroscopy was used to evaluate the surface functional groups in the immobilization procedure. FT-IR spectra were recorded on a Perkin-Elmer spectrometer using a KBr method. The thickness of the GONS was confirmed by atomic force microscopy (AFM; Agilent 5500, Santa Clara, CA, USA) measurements. The average diameters of GONSs were obtained using a dynamic light scattering photometers (ELS-8000, Otsuka Electronics Co., Ltd.) at room temperature.

5.3 Results and Discussion

The amount of trypsin immobilized on the GONS was calculated to be about 1.9 mg mg⁻¹, which was more than about 22 times and 7.6 times higher than the amounts immobilized on the magnetic nanoparticles (diameter: 50 nm) prepared by Deng (86 μgmg⁻¹)³ and the nanodiamond particles (diameter: 310 nm) prepared by Lu (250 μgmg⁻¹)⁴ respectively. This large trypsin content on the GONS is a result of its high surface ratio (about 2600m² g⁻¹ as GO sheets)¹⁶ and large content of functional groups (carboxylic acid groups) on the surface.¹⁸

Figure 5-1 shows the FT-IR spectra of the GONS, trypsin powder, and trypsin-immobilized GONS (trypsinGONS), obtained using a FT-IR spectrometer. The characteristic IR features of GO indicate the presence of abundant oxygen-containing functional groups on the GO surface. The characteristic bands at 1045, 1380, 1642, and 1724 cm⁻¹ correspond to COC stretching vibrations, OH deformation of the COH groups, the C=C stretching mode of the sp² C network, and the C=O stretching vibrations of the COOH group, respectively (Figure 5-1a). After trypsin was immobilized on the GONS, the C=O stretching vibrations of the COOH group (1724 cm⁻¹) disappeared, but the functional groups of trypsin,

such as amide I (C=O stretching vibration of R-CONHR') at 1639 cm^{-1} and amide II (N-H bending vibration of R-NHR' and its NH stretching vibration) at 1535 and 3300 cm^{-1} (Figure 5-1b) emerged in the trypsinGONS spectrum (Figure 5-1c). These results suggest that trypsin macromolecules were covalently immobilized on the GONS surface by coupling with the carboxy groups of the GONS via amide bonds.

The surface morphologies of GONS and trypsinGONS are shown in Figures 5-2a and 5-2b, as AFM images in tapping mode. The thickness of the GONS was about 11.5 nm (Figure 5-2a). The measured thickness is almost the same as those already reported for GO single nanosheets (about 1.0 nm).¹⁸ The high dispersion activity of a GONS in water is a result of its high hydrophilicity. In contrast, trypsinGONSs had various thicknesses ranging from 4 to 8 nm (Figure 5-2b). The diameter of trypsin in aqueous solution is about 2.8 to 5 nm.²¹ The GO nanosheet thickness increased from 1 to 1.5 nm to 48nm with immobilization of trypsin from 0 to 1.9mg per mg-GONS. In the analysis of the GONS size by dynamic light scattering, the average diameter of the trypsinGONSs was about 1.9 times the average GONS diameter (Table 5-1). The results suggest that trypsin macromolecules were immobilized on both sides of the GONS surface. This is consistent with the FT-IR results.

The catalytic kinetics of the trypsinGONS and free trypsin were investigated at 37 °C and pH 7.0. Various concentrations (2.0-20.0 mgmL^{-1}) of casein solution were used as the substrate. The protease activity of trypsin against casein was determined using Keay's method.²² One unit (U) of enzyme activity is the quantity of enzyme that releases 1.0 μg of tyrosine per minute. The affinities of trypsinGONS and trypsin against casein were determined from the Michaelis constant (K_m) and the maximum effective velocity (V_{max}). The K_m values of free trypsin and trypsin-GONS were found to be 65 and 125 mgmL^{-1} , respectively, and those of V_{max} were 680

and $360\mu\text{gmin}^{-1}$, respectively. In the experiments, increases in K_m and decreases in V_{max} are generally observed for enzyme immobilization, as reported in the literature.⁴ The apparent K_m value of trypsin-GONS was about 1.92 times higher than that of free trypsin. This increase in the apparent K_m value might be caused by structural changes in the enzyme induced by the immobilization of trypsin and reduced accessibility of the substrate to the active sites of the immobilized enzyme.²³ The initial activities of free trypsin and trypsin-GONS in the hydrolysis of casein (1.5 mgmL^{-1}) were about 3.1×10^3 and $2.2 \times 10^3\text{Umg}^{-1}$ (or $1.0 \times 10^3\text{U}$ per mg-dried-nanosheet), respectively, which were better than those obtained using other methods for immobilizing enzymes.²⁴ These results mean that the catalytic function of trypsin was not impaired significantly by immobilization on a GONS.

The properties of trypsin-GONS and free trypsin were compared in order to study the actual stabilization of immobilized trypsin. The stability of trypsin was determined by measuring its residual activity after exposure to various temperatures for given time intervals of several hours. Figure 5-3a shows the effect of the incubation temperature of free trypsin on the stability of its protease activity. After treatment at $5\text{ }^\circ\text{C}$ for 2 h, the free trypsin still retained 96% of its initial activity. However, the residual activity of free trypsin depended significantly on the treatment temperature. Its residual activity decreased from 96% to 4% with increasing treatment temperature from 5 to $50\text{ }^\circ\text{C}$ for 2h. Figure 3b shows the results of a comparison of the thermal stabilities of free trypsin and trypsin-GONS at $50\text{ }^\circ\text{C}$. The trypsin-GONS was inactivated slowly in comparison with free trypsin. After heat treatment at $50\text{ }^\circ\text{C}$ for 6 h, trypsin-GONS retained 80% of its initial activity and still retained 60% even after 12 h. However, the residual activities of free trypsin were 8% and 4% after 1 and 6 h, respectively, at $50\text{ }^\circ\text{C}$. The denatured stability of trypsin-GONS and that of free trypsin were compared after ethanol treatment. As shown in

Figure 5-3c, the denatured stability of the trypsin-GONS was always higher than that of free trypsin for an ethanol concentration of 10 to 50 vol%. The residual activity of free trypsin decreased from 75% to 2% with increasing ethanol concentration from 10 to 50 vol%. In contrast, trypsin-GONS still retained 78% of its initial activity even after treatment with 50 vol% ethanol at 37 °C for 30min. These results demonstrate that the immobilization of an enzyme on a GONS increases its stability. Trypsin-immobilized magnetic nanoparticles³ and trypsin-immobilized nanodiamond particles⁴ have already been used to increase the proteolytic stability of trypsin. However, the covalent method is more complicated and these nanoparticles are expensive. In contrast, the immobilization of trypsin on GO sheets, which have many functional groups on their surfaces, is simple, handling is easy, and the GO sheets are very cheap.

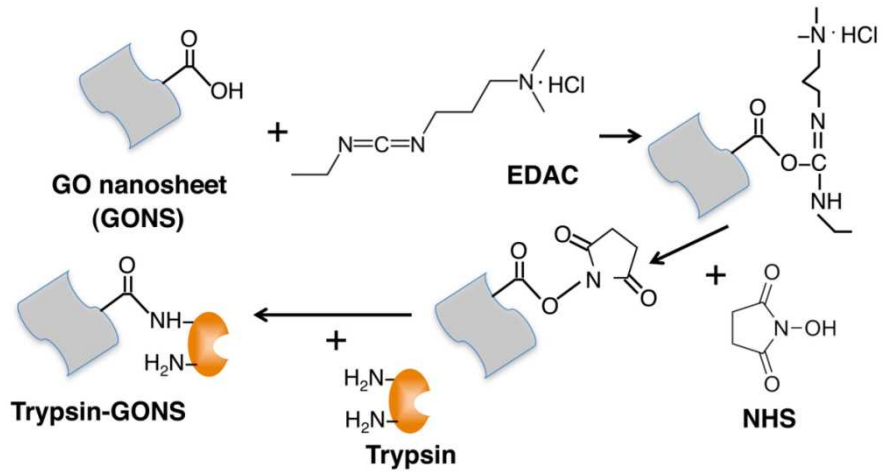
5.4 Conclusion

We have developed a novel enzyme-immobilized GONS using a one-step and natural reaction. Trypsin was successfully immobilized on the GONS by diimide-activated amidation. The amount of trypsin immobilized on the GONS (1.9 mg mg⁻¹) was higher than those immobilized on nanoparticle supports. A large amount of trypsin was immobilized on the GONS surface as a result of its high surface ratio and its large content of functional (carboxy) groups. Furthermore, compared with free trypsin, trypsin-GONS showed higher stability to temperature and ethanol. This high stability of trypsin-GONS is a result of stabilization of weak intermolecular forces and prevention of enzyme autolysis when trypsin-GONS is sufficiently dispersed in solution. The whole amidation process was conducted within only 60min, which is easy to scale up at a low cost. These results are expected to open up new applications of GONSs in proteomics.

References

- (1) A. Monzo, E. Sperling, A. Guttman, *TrAC, Trends Anal. Chem.*, 2009, 28, 854.
- (2) K. Sangeetha, T. E. Abraham, *J. Mol. Catal. B: Enzym.*, 2006, 38, 171.
- (3) J. Liu, S. Lin, D. Qi, C. Deng, P. Yang, X. Zhang, *J. Chromatogr. A* 2007, 1176, 169.
- (4) L. Wei, W. Zhang, H. Lu, P. Yang, *Talanta.*, 2010, 80, 1298.
- (5) A. G. Kumar, K. Perinbam, P. Kamatchi, N. Nagesh, G. Sekaran, *Bioresour. Technol.*, 2010, 101, 1377.
- (6) J. Zhao, Y. Wang, G. Luo, S. Zhu, *Bioresour. Technol.*, 2011, 102, 529.
- (7) E. Yilmaz, K. Can, M. Sezgin, M. Yilmaz, *Bioresour. Technol.*, 2011, 102, 499.
- (8) G. D. Altun, S. A. Cetinus, *Food Chem.*, 2007, 100, 964.
- (9) H.-M. Ding, L. Shao, R.-J. Liu, Q.-G. Xiao, J.-F. Chen, *J. Colloid Interface Sci.*, 2005, 290, 102.
- (10) J. Li, J. Wang, V. G. Gavalas, D. A. Atwood, L. G. Bachas, *Nano Lett.*, 2003, 3, 55.
- (11) C. Rocha, M. P. Gonçalves, J. A. Teixeira, *Process Biochem.*, 2011, 46, 505.
- (12) S. Stankovich, D. A. Dikin, G. H. B. Dommett, K. M. Kohlhaas, E. J. Zimney, E. A. Stach, R. D. Piner, S. T. Nguyen, R. S. Ruoff, *Nature.*, 2006, 442, 282.
- (13) S. Park, R. S. Ruoff, *Nat. Nanotechnol.*, 2009, 4, 217.
- (14) K. Wakabayashi, C. Pierre, D. A. Dikin, R. S. Ruoff, T. Ramanathan, L. C. Brinson, J. M. Torkelson, *Macromolecules.*, 2008, 41, 1905.
- (15) H. Hu, X. Wang, J. Wang, F. Liu, M. Zhang, C. Xu, *Appl. Surf. Sci.*, 2011, 257, 2637.
- (16) T. Ramanathan, A. A. Abdala, S. Stankovich, D. A. Dikin, M. Herrera-Alonso, R. D. Piner, D. H. Adamson, H. C. Schniepp, X. Chen, R. S. Ruoff, S. T. Nguyen, I. A. Aksay, R. K. Prud'Homme, L. C. Brinson, *Nat. Nanotechnol.*, 2008, 3, 327.

- (17) W. S. Hummers, Jr., R. E. Offeman, *J. Am. Chem. Soc.*, 1958, 80, 1339.
- (18) Y. Matsumoto, M. Koinuma, S. Y. Kim, Y. Watanabe, T. Taniguchi, K. Hatakeyama, H. Tateishi, S. Ida, *ACS Appl. Mater. Interfaces.*, 2010, 2, 3461.
- (19) N. Nakajima, Y. Ikeda, *Bioconjugate Chem.*, 1995, 6, 123.
- (20) W. Huang, S. Taylor, K. Fu, Y. Lin, D. Zhang, T. W. Hanks, A. M. Rao, Y.-P. Sun, *Nano Lett.*, 2002, 2, 311.
- (21) K. Nozawa, A. Shoji, M. Sugawara, *Supramol. Chem.*, 2010, 22, 389.
- (22) L. Keay, B. S. Wildi, *Biotechnol. Bioeng.*, 1970, 12, 179.
- (23) J. F. Kennedy, E. H. M. Melo, K. Jumel, *Chem. Eng. Prog.*, 1990, 86, 81.
- (24) H. A. Chase, Y. Yang, *Biotechnol. Appl. Biochem.*, 1998, 27, 205.



Scheme 5-1. Immobilization of trypsin on GONS by diimideactivated amidation.

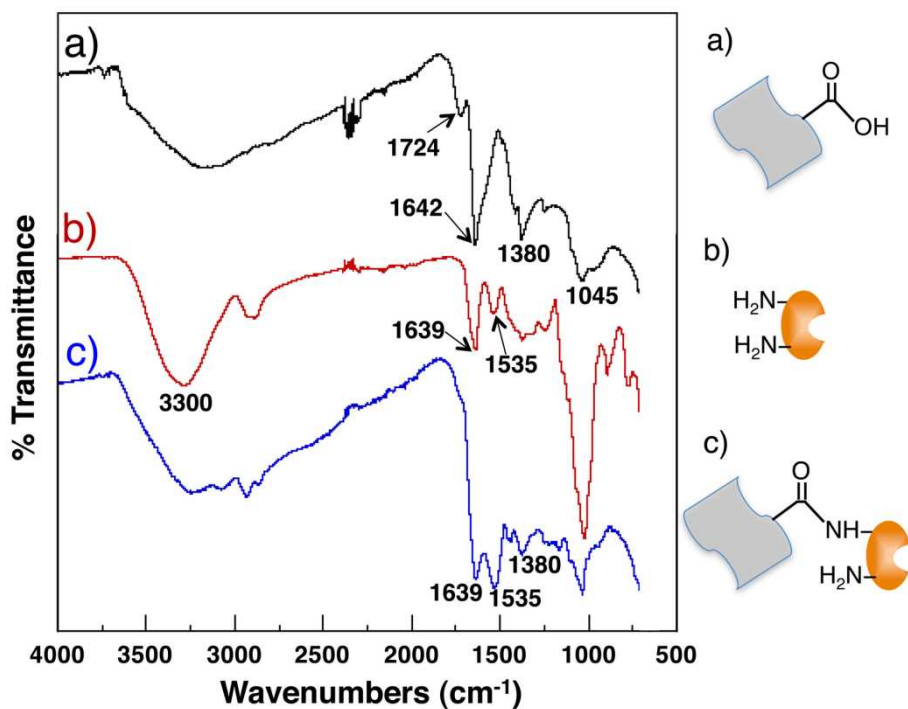


Figure 5-1. FT-IR spectra of (a) GONS, (b) trypsin, and (c) trypsinGONS. The immobilization of trypsin onto GONS was achieved by diimide-activated amidation with 5mL of GONS dispersion (500 gmL⁻¹) and 5mg of trypsin at pH 6.

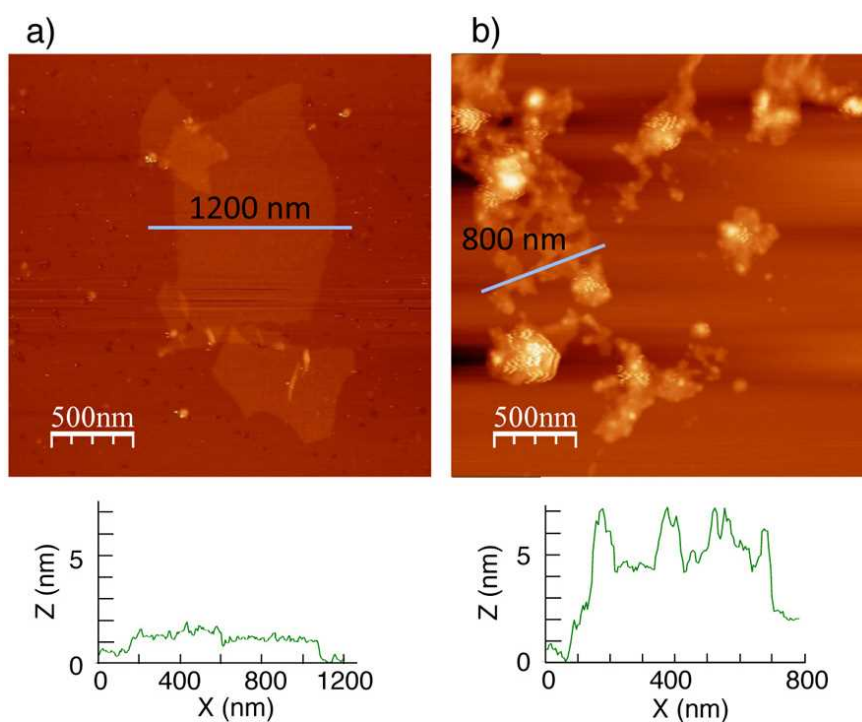


Figure 5-2. Tapping-mode AFM images of (a) GONS and (b) trypsinGONS films. The nanosheet films were prepared by dropping a nanosheet suspension (pH 6.0) onto a mica surface.

Table 5-1. Average diameters of GONS and trypsin-immobilized GONS by GONS-size analysis using dynamic light scattering

GONS (500 mg mL ⁻¹ in water) nm (±)	Trypsin-GONS (2.2×10 ³ U mg ⁻¹ in water) nm (±)
1064 (±209)	2034 (±378)

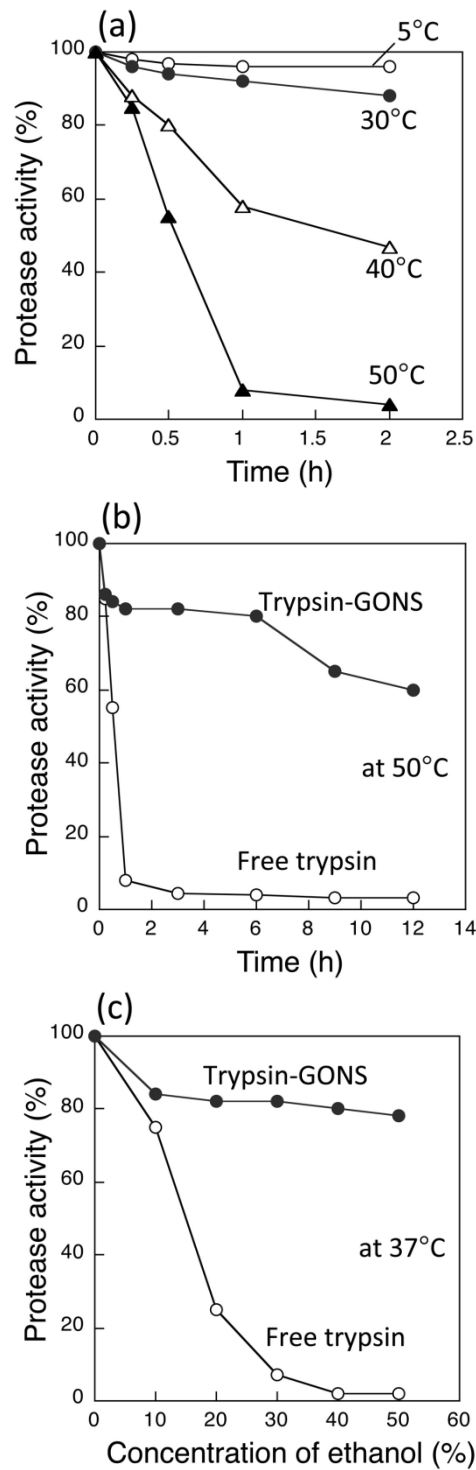


Figure 5-3. Properties of trypsin under various conditions (a) thermal stability of free trypsin at 5–50°C; (b) thermal stabilities of free trypsin and trypsin-GONS at 50 °C for 0.5–12 h; (c) chemical stabilities of free trypsin and trypsin-GONS (37 °C, 30 min). Initial activity: free trypsin (3.1×10^3 U mg^{-1}), trypsin-GONS (2.2×10^3 U mg^{-1}).

CHAPTER-VI

General Conclusion

Nanosheets have been extensively investigated for the fabrication of ultrathin devices. For example, graphene is a potential nanosheet material that can replace Si devices in the near future. Moreover, many groups have reported layered films reassembled from nanosheets because of the expectation for various applications such as photocatalysts, batteries, semiconductor devices and optical devices.

In the present study, we investigated the adsorption behavior of nanosheets, synthesis of novel nanosheets and photoluminescence properties of nanosheets.

The summary of each chapter is described as follows:

- **Chapter 1** narrated the general background of nanosheets, aim of the present study, general properties of nanosheets and application of nanosheets.

- **Chapter 2** presented that intense emissions of Ln³⁺ ions (Eu³⁺ and Tb³⁺) adsorbed on TiO (Ti_{1.825}O₄) and NbO (Nb₆O₁₇) nanosheets were observed. This photoluminescence results from the energy transfer from the band gap excitation of the nanosheets to the adsorbed Ln³⁺. Co-adsorbed H₂O increased the emission intensities of the adsorbed Ln³⁺. Hydrogen-bonding networks between O²⁻ ions of the nanosheet surface and the adsorbed H₂O surrounding Ln³⁺ will promote the energy transfer for Ln³⁺/MO. The intensity increased in D₂O because of the decrease of phonon effect of co-adsorbed water molecules. Consequently, the energy transfer promotion by the co-adsorbed H₂O is stronger than the phonon effect, leading to the increase of the emission intensity in high humidity and water. The emission intensity of the Eu³⁺/TiO and the Tb³⁺/NbO, while Co²⁺ and Ag⁺ addition decreased the emission intensity because the photoproduced electron and hole in the nanosheets are consumed by photoelectrochemical reactions.

• **Chapter 3** presented that we succeeded a new easy preparation method for titanium oxide nanosheets by exfoliating layered oxide ($K_{1.1}H_{0.9}Ti_2O_5 \cdot nH_2O$) precursors prepared by a solution process under mild conditions (i.e., room temperature ~ 80 °C). The concentrated nanosheet solutions were easily obtained when the layered oxide precursors were prepared in the presence of SDS, suggesting that the mass production of titanium oxide nanosheets by a low-cost process, which is important for the practical use of these nanosheets, is feasible. The drastic and specific enhancement of Eu^{3+} emission by energy transfer from the $Ti_2O_5^{2-}$ nanosheets occurred in the solution state. To the best of our knowledge, this study represents the first report of energy-transfer PL in an aqueous solution. The remarkable and specific enhancement of the emission by the energy transfer was very useful for a trace analysis of Eu^{3+} .

• **Chapter 4** presented that we successfully synthesized NIR luminescent metal oxide nanosheets for the first time by the exfoliation of $KLa_{1-x}Nd_xNb_2O_7$ layered perovskite. The colloidal nanosheets afford 1060-nm luminescence resulting from ${}^4F_{3/2} \rightarrow {}^4I_{11/2}$ (Nd^{3+}) transitions upon excitation at 808 nm. Surface modification of nanosheets by APTES and PAA resulted in six-fold enhanced luminescent intensity while maintaining a high colloidal stability. Our study demonstrated that Nd^{3+} -doped nanosheets exhibit NIR luminescent properties with their large tunability depending on surface states, which will lead to the development of smart bioimaging probes and bioanalytical sensors.

• **Chapter 5** presented that we have developed a novel enzyme-immobilized GONS using a one-step and natural reaction. Trypsin was successfully immobilized on the GONS by diimide-activated amidation. A large amount of trypsin was immobilized on the GONS surface as a result of its high surface ratio and its large content of functional groups. Furthermore, compared with free trypsin, trypsin-GONS showed higher stability to temperature and ethanol.

This high stability of trypsin-GONS is a result of stabilization of weak intermolecular forces and prevention of enzyme autolysis when trypsin-GONS is sufficiently dispersed in solution. These results are expected to open up new applications of GONSs in proteomics.

We believe that nanosheets have the potential to create many new materials and devices. Development of application incorporating nanosheets to be used in the next generation of products, such as solar cell, fuel cell, and biosensor.

ACKNOWLEDGEMENTS

I would like to express my sincerest thanks to **Professor Yasumichi Matsumoto** for his invaluable comments and suggestions, and his encouragement through the period of this study.

I would also like to thank to other members of my committee: Professor Masato Machida, Professor Seiji Kurihara, Professor Masashi Kunitake, and Dr. Michio Koinuma.

I would like to express my appreciation to Assistant Professor Takaaki Taniguchi and Associate Professor Shintaro Ida, for their advices, and encouragements.

I would like to express my deepest appreciation to Associate Professor Masayo Sakata, for her advices, teaching me and encouragement in my study life.

I would like to express my deepest appreciation to Ms. Kiyomi Tahara Secretary in this laboratory, for her advices and assistance.

I am deeply thankful to Mr. Tomoaki Murakami, Ms. Yuki Nojiri, Mr. Yosuke Tokita, Mr. Kotaro Koga, Mr. Kazuto Hatakeyama, Mr. Hikaru Tateishi, Ms. Ayame Oki, Ms. Yuko Fukunaga, Ms. Yui Fukushima, and Ms. Chikako Ogata for their encouragement and assistance.

I am also thankful to students in Matsumoto Laboratory.

Finally, I deeply thank my parents and brother for their support and hearty encouragement through my student life.

Asami Funatsu

Kumamoto

2013